VTEM™plus

REPORT ON A HELICOPTER-BORNE VERSATILE TIME DOMAIN ELECTROMAGNETIC (VTEM™ Plus) AND HORIZONTAL MAGNETIC GRADIOMETER GEOPHYSICAL SURVEY

PROJECT: WARWICK-LOW K BARRIER
LOCATION: JAMESTOWN NORTH DAKOTA
FOR: NORTH DAKOTA STATE WATER COMMISSION
SURVEY FLOWN: OCTOBER 2016
PROJECT: GL160299

GEOTECH
AIRBORNE GEOPHYSICAL SURVEYS

TABLE OF CONTENTS

LIST OF FIGURES

LIST OF TABLES

APPENDICES

EXECUTIVE SUMMARY

WARWICK-LOW K BARRIER
JAMESTOWN, NORTH DAKOTA

During October 22nd to October 24th 2016 Geotech Ltd. carried out a helicopter-borne geophysical survey over the Warwick-Low K Barrier Block situated near Jamestown, North Dakota.

Principal geophysical sensors included a versatile time domain electromagnetic (VTEM™plus) system and a horizontal magnetic gradiometer with two caesium sensors. Ancillary equipment included two GPS navigation systems, a radar altimeter, a laser altimeter and a gyroscopic inclinometer. A total of 112 line-kilometres of geophysical data were acquired during the survey.

In-field data quality assurance and preliminary processing were carried out on a daily basis during the acquisition phase. Preliminary and final data processing, including generation of final digital data and map products were undertaken from the office of Geotech Ltd. in Aurora, Ontario.

The processed survey results are presented as the following maps:

- Electromagnetic stacked profiles of the B-field Z Component,
- Electromagnetic stacked profiles of dB/dt Z Components,
- B-Field Z Component Channel grid,
- Total Magnetic Intensity (TMI),
- Magnetic Total Horizontal Gradient,
- Magnetic Tilt-Angle Derivative

The final processed data was inverted to create 1D resistivity models over the entire survey block. The inversion results were effective at mapping what appears to be the Spiritwood-Warwick aquifer in the north-to-south direction and an additional aquifer in the northeast-to-southwest direction. Both of these aquifers appear to intersect near the middle of the survey block. These results are presented as:

- Planar resistivity depth slices at 10 metre intervals
- Cross-sectional resistivity models for each flight and tie line
- 3D gridded voxel composed from each 1D inversion model

Digital data includes all electromagnetic and magnetic products, plus ancillary data including the waveform and all inversion modeling products.

The survey report describes the procedures for data acquisition, processing, final image presentation, inversion modeling, and the specifications for the digital data set.

Project GL160299
VTEM™plus Report on Airborne Geophysical Survey
for North Dakota State Water Commission

iii

GEOTECH
AIRBORNE GEOPHYSICAL SURVEYS

1. INTRODUCTION

1.1 GENERAL CONSIDERATIONS

Geotech Ltd. performed a helicopter-borne geophysical survey over the Warwick-Low K Barrier Block situated near Jamestown, North Dakota (Figure 1 & Figure 2).

David Hisz represented North Dakota State Water Commission during the data acquisition, data processing, and data modeling phases of this project

The geophysical surveys consisted of helicopter borne EM using the versatile time-domain electromagnetic (VTEM) plus system with Full-Waveform processing. Measurements consisted of Vertical (Z), In-line Horizontal (X), and Cross-line Horizontal (Y) components of the EM fields using induction coils and the aeromagnetic total field using two caesium magnetometers. A total of 112 line-km of geophysical data were acquired during the survey. The VTEM plus system with Full-Waveform processing was selected for this project due to previous success it had in mapping the Spiritwood aquifer in southern Manitoba[1].

The crew was based out of Jamestown (Figure 2) in North Dakota for the acquisition phase of the survey. Survey flying started on October 4th and was completed on October 22nd, 2016.

Figure 1: Survey location

---

[1] Prikhodko et al. 2013, Recent AEM Case Study Examples Using a Full Waveform Time-Domain System for Near-Surface Applications: SAGEEP Conference 2013.

Data quality control and quality assurance, and preliminary data processing were carried out on a daily basis during the acquisition phase of the project. Final data processing followed immediately after the end of the survey. Final reporting, data presentation, data modeling and archiving were completed from the Aurora office of Geotech Ltd. in March, 2017. The final models and mapping products proved that VTEM was effective at mapping the Spiritwood aquifer an additional aquifer which intersects it within the survey block.

1.2 SURVEY AND SYSTEM SPECIFICATIONS

The survey area is located east of Jamestown, North Dakota (Figure 2).
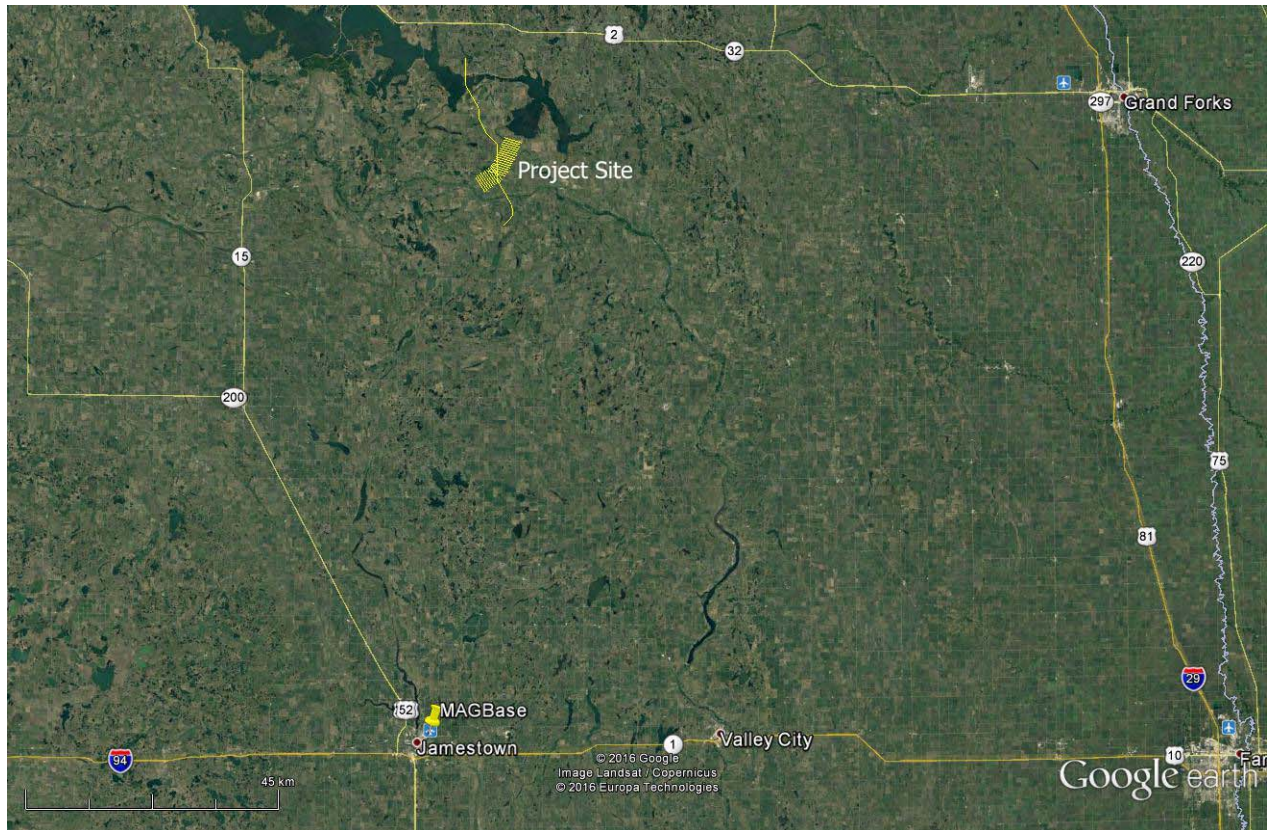
Figure 2: Survey area location on Google Earth.

The survey areas were both flown in a southeast to northwest (N 107° E azimuth & N 145° E azimuth) direction with traverse line spacing of 400 metres as depicted in Figure 3. Tie lines were neither flown nor planned.

For more detailed information on the flight spacing and direction see Table 1.

1.3   TOPOGRAPHIC RELIEF AND CULTURAL FEATURES

Topographically, the survey area exhibits a shallow relief with an elevation ranging from 440 to 452 metres above mean sea level over an area of 36 square kilometres (Figure 3).

There are various rivers and streams running through the survey area which connect various lakes. There are visible signs of culture such as roads, railways and settlements located in and around the survey area.

Figure 3: Flight path over a Google Earth Image.

2. DATA ACQUISITION

2.1 SURVEY AREA

The survey area (see Figure 3 and Appendix A) and general flight specifications are as follows:

Table 1: Survey Specifications

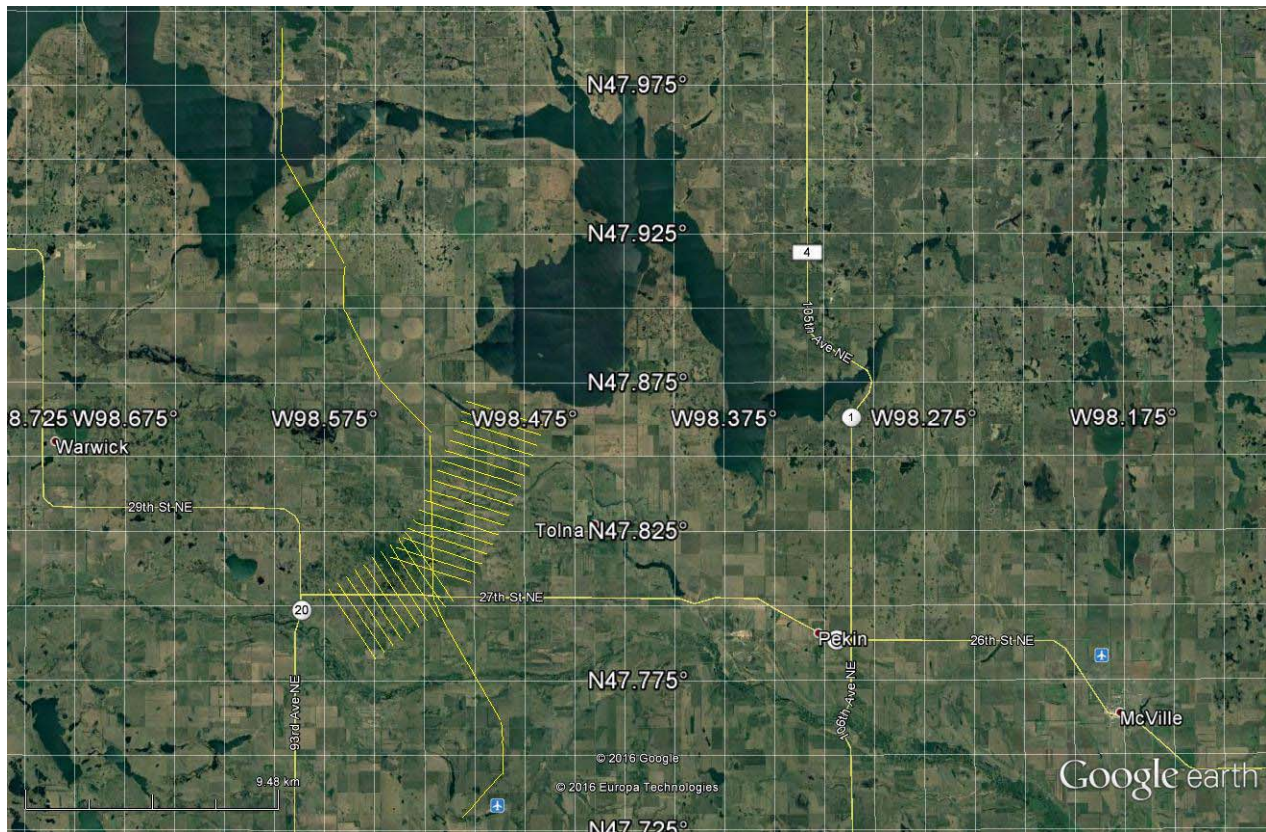| Survey block	Line spacing (m)	Area (Km^2)	Planned[2] Line-km	Actual Line-km	Flight direction	Line numbers
Area 1	Traverse: 400		51	53.4	N 107° E / N 287° E	L1000 – L1161
Area 2	Traverse: 400	36	30	31.4	N 145° E / N 325° E	L1190 – L1280
Lines	n/a		31	31.9	n/a	L1300 – L1380
TOTAL		36	112	116.7		

Survey area boundaries co-ordinates are provided in Appendix B.

2.2 SURVEY OPERATIONS

Survey operations were based out of Jamestown in North Dakota from October 22nd until 24th 2016. The following table shows the timing of the flying.

Table 2: Survey schedule

Date	Flight #	Flown km	Block	Crew location	Comments
22-Oct-2016	1	52	A1/2	Jamestown, NorthDakota	52km flown
23-Oct-2016				Jamestown, NorthDakota	No production due to weather
24-Oct-2016	2	64	A1/2, Line 3	Jamestown, NorthDakota	Remaining kms were flown- flying complete

---

[2] Note: Actual Line kilometres represent the total line kilometres in the final database. These line-km normally exceed the Planned Line-km, as indicated in the survey NAV files.

2.3   PROCEDURES

The on board operator was responsible for monitoring the system integrity. He also maintained a detailed flight log during the survey, tracking the times of the flight as well as any unusual geophysical or topographic features.

On return of the aircrew to the base camp the survey data was transferred from a compact flash card (PCMCIA) to the data processing computer. The data were then uploaded via ftp to the Geotech office in Aurora for daily quality assurance and quality control by qualified personnel.

2.4   AIRCRAFT AND EQUIPMENT

2.4.1   SURVEY AIRCRAFT

The survey was flown using a Eurocopter Aerospatiale (Astar) 350 B3 helicopter, registration C-FVTM. The helicopter is owned and operated by Geotech Aviation. Installation of the geophysical and ancillary equipment was carried out by a Geotech Ltd crew.

2.4.2   ELECTROMAGNETIC SYSTEM

The electromagnetic system was a Geotech Time Domain EM (VTEM™plus) full receiver-waveform streamed data recorded system. The "full waveform VTEM system" uses the streamed half-cycle recording of transmitter and receiver waveforms to obtain a complete system response calibration throughout the entire survey flight. This system configuration has been proven successful in mapping buried aquifers on previous project including the mapping of the Spiritwood aquifer in southern Manitoba (Prikhodko et al, 2013). VTEM with the Serial number 7 had been used for the survey. The VTEM™ transmitter current waveform is shown diagrammatically in Figure 4.

The VTEM™ Receiver and transmitter coils were in concentric-coplanar and Z-direction oriented configuration. The receiver system for the project also included coincident-coaxial X-direction and Y-direction coils to measure the in-line and cross-line dB/dt and calculate B-Field responses, respectively. The transmitter-receiver loop was towed at a mean distance of 38 metres below the aircraft as shown in Figure 5.
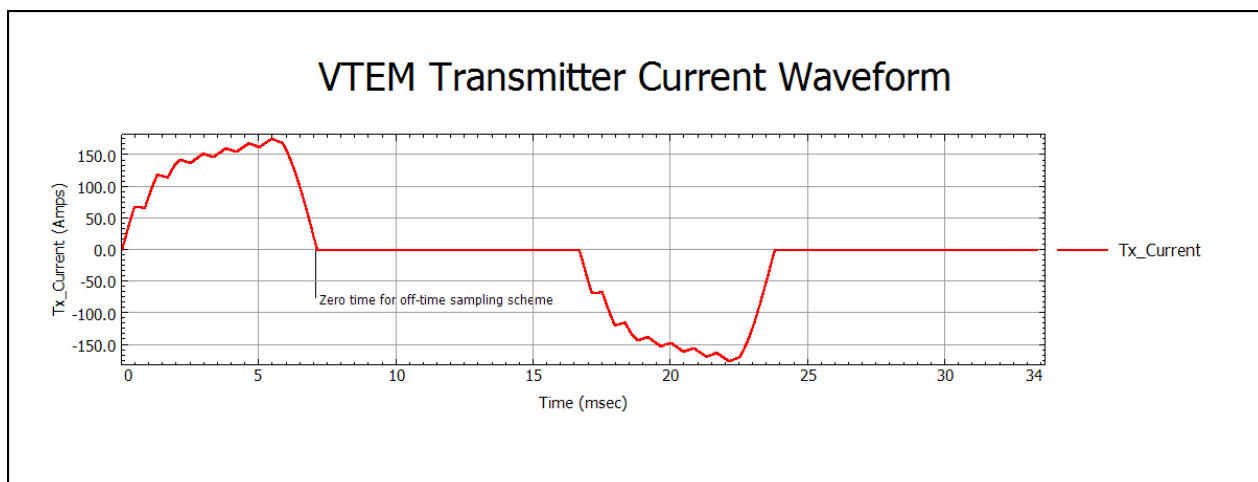

Figure 4: VTEM™ Transmitter Current Waveform

The VTEM™ decay sampling scheme is shown in Table 3 below. Forty-four time measurement gates were used for the final data processing in the range from 0.021 to 8.083 msec. Zero time for the off-time sampling scheme is equal to the current pulse width and is defined as the time near the end of the turn-off ramp where the dI/dt waveform falls to 1/2 of its peak value.

Table 3: Off-Time Decay Sampling Scheme

VTEM™ Decay Sampling Scheme				
Index	Start	End	Middle	Width
Milliseconds				
4	0.018	0.023	0.021	0.005
5	0.023	0.029	0.026	0.005
6	0.029	0.034	0.031	0.005
7	0.034	0.039	0.036	0.005
8	0.039	0.045	0.042	0.006
9	0.045	0.051	0.048	0.007
10	0.051	0.059	0.055	0.008
11	0.059	0.068	0.063	0.009
12	0.068	0.078	0.073	0.010
13	0.078	0.090	0.083	0.012
14	0.090	0.103	0.096	0.013
15	0.103	0.118	0.110	0.015
16	0.118	0.136	0.126	0.018
17	0.136	0.156	0.145	0.020
18	0.156	0.179	0.167	0.023
19	0.179	0.206	0.192	0.027
20	0.206	0.236	0.220	0.030
21	0.236	0.271	0.253	0.035
22	0.271	0.312	0.290	0.040
23	0.312	0.358	0.333	0.046
24	0.358	0.411	0.383	0.053
25	0.411	0.472	0.440	0.061
26	0.472	0.543	0.505	0.070
27	0.543	0.623	0.580	0.081
28	0.623	0.716	0.667	0.093
29	0.716	0.823	0.766	0.107
30	0.823	0.945	0.880	0.122
31	0.945	1.086	1.010	0.141
32	1.086	1.247	1.161	0.161
33	1.247	1.432	1.333	0.185
34	1.432	1.646	1.531	0.214
35	1.646	1.891	1.760	0.245
36	1.891	2.172	2.021	0.281
37	2.172	2.495	2.323	0.323
38	2.495	2.865	2.667	0.370

VTEM™ Decay Sampling Scheme				
Index	Start	End	Middle	Width
Milliseconds				
39	2.865	3.292	3.063	0.427
40	3.292	3.781	3.521	0.490
41	3.781	4.341	4.042	0.560
42	4.341	4.987	4.641	0.646
43	4.987	5.729	5.333	0.742
44	5.729	6.581	6.125	0.852
45	6.581	7.560	7.036	0.979
46	7.560	8.685	8.083	1.125

Z Component: 4 - 46 time gates
X Component: 20 - 46 time gates
Y Component: 20 - 46 time gates

VTEM™ system specifications:

| Transmitter	Receiver
• Transmitter loop diameter: 26 m • Number of turns: 4 • Effective Transmitter loop area: 2123.7 m^2 • Transmitter base frequency: 30 Hz • Peak current: 172 A • Pulse width: 7.11 ms • Waveform shape: Bi-polar trapezoid • Peak dipole moment: 365,276 nIA • Average transmitter-receiver loop terrain clearance: 34 metres above the ground	• X Coil diameter: 0.32 m • Number of turns: 245 • Effective coil area: 19.69 m^2 • Y Coil diameter: 0.32 m • Number of turns: 245 • Effective coil area: 19.69 m^2 • Z-Coil diameter: 1.2 m • Number of turns: 100 • Effective coil area: 113.04 m^2
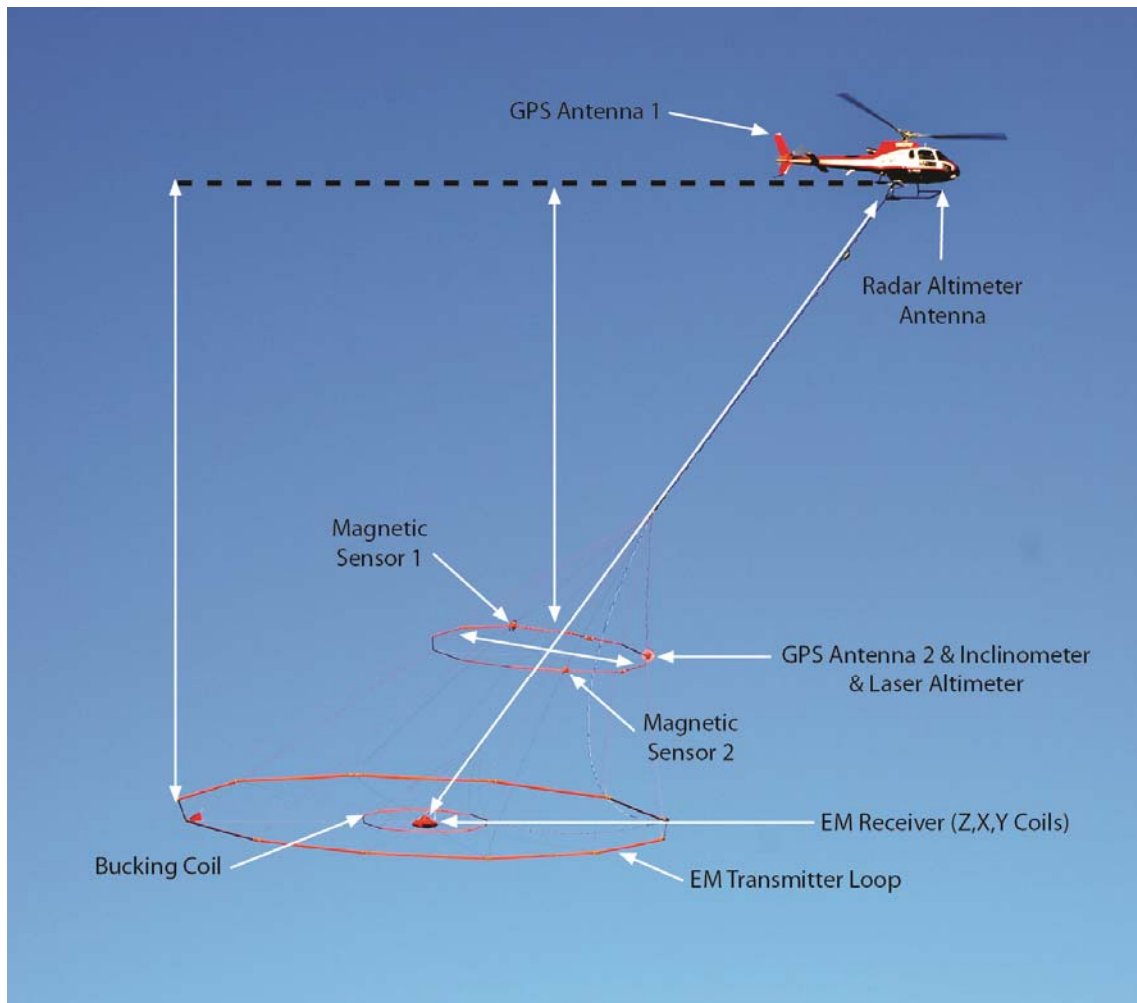
Figure 5: VTEM™Plus System Configuration.

2.4.3   Full waveform vtem™ sensor calibration

The calibration is performed with the completely assembled VTEM system connected to the helicopter at the survey site on the ground. Measurements of the half-cycles are collected and used to calculate a sensor calibration consisting of a single stacked half-cycle waveform. The purpose of the stacking is to attenuate natural and man-made magnetic signals, leaving only the response to the calibration signal. The stacked half-cycle allows the transfer functions between the receiver and data acquisition system, $H_D(\omega)$, and current sensor and data acquisition system, $H_R(\omega)$, to be determined. These transfer functions are used as a part of the system response correction during processing to correct the half-cycle waveforms and data acquired on a survey flight to a common transfer function:

$$D(\omega) = [H_C(\omega)/H_D(\omega)]\, D_R(\omega)$$
$$A(\omega) = [H_C(\omega)/H_R(\omega)]\, A_R(\omega)$$

where $H_C(\omega)$ is the common transfer function, and $D_R(\omega)$ and $A_R(\omega)$ are the FFT's of the raw receiver and current sensor responses recorded by the data acquisition system.

This process allows for the receiver response, $R(\omega)$, to become independent of the sensor characteristics determined by the transfer functions $H_D(\omega)$ and $H_R(\omega)$ and acts similar to a deconvolution of the data.

$$R(\omega) = \frac{D(\omega)I(\omega)}{A(\omega)}$$

where, $D(\omega)$ is the FFT of the actual receiver data sample $D(t)$, $I(\omega)$ is the FFT of a reference or "Ideal waveform" and $A(\omega)$ is the FFT of the actual waveform.

2.4.4   Horizontal Magnetic Gradiometer

The horizontal magnetic gradiometer consists of two Geometrics split-beam field magnetic sensors with a sampling interval of 0.1 seconds. These sensors are mounted 12.5 metres apart on a separate loop, 9 metres above the Transmitter-receiver loop. A GPS antenna and Gyro Inclinometer is installed on the separate loop to accurately record the tilt and position of the magnetic gradiomag bird.

2.4.5   GPS Navigation System

The navigation system used was a Geotech PC104 based navigation system utilizing a NovAtel's WAAS (Wide Area Augmentation System) enabled GPS receiver, Geotech navigate software, a full screen display with controls in front of the pilot to direct the flight and a NovAtel GPS antenna mounted on the helicopter tail (Figure 5). As many as 11 GPS and two WAAS satellites may be monitored at any one time. The positional accuracy or circular error probability (CEP) is 1.8 m, with WAAS active, it is 1.0 m. The co-ordinates of the survey area were set-up prior to the survey and the information was fed into the airborne navigation system. The second GPS antenna is installed on the additional magnetic loop together with Gyro Inclinometer.

2.4.6   GPS - Magnetic-Gradiometer Loop

A NovAtel GPS antenna was installed on the front centre of the magnetic gradiometer loop to accurately record the position of the loop (Figure 5). GPS data were sampled every 0.1 seconds. The

final GPS coordinates were differentially corrected by post-processing the gradiometer loop data along with GPS data obtained simultaneously from a base station setup nearby the survey area. Final horizontal coordinates are referenced to WGS84 UTM zone 14N and the height is referenced to the geoid. The positional accuracy or circular error probability (CEP) is 1.0 m.

2.4.7 INCLINOMETER – MAGNETIC GRADIOMETER LOOP

An Anlalog Devices ADIS16405 gyroscopic inclinometer was installed on the magnetic gradiometer loop (Figure 5) to accurately record the orientation of the loop with a sampling interval of 0.1 seconds.

2.4.8 RADAR ALTIMETER

A Terra TRA 3000/TRI 40 radar altimeter was used to record terrain clearance. The antenna was mounted beneath the bubble of the helicopter cockpit (Figure 5).

2.4.9 LASER ALTIMETER

A Schmitt Industries AR300 laser altimeter was used which has an altitude range 0.5 to 300m and accuracy ±5cm. The laser altimeter was located at the front of the horizontal magnetic gradient loop with a GPS antenna and inclinometer and the data was sampled at an interval of 0.2 seconds.

2.4.10 VIDEO CAMERA

A Garmin VIRB®X camera was used which captures high-definition, wide-angle footage at 1080p30, 12 megapixel photos at up to 10 frames per second.

2.4.11 DIGITAL ACQUISITION SYSTEM

A Geotech data acquisition system recorded the digital survey data on an internal compact flash card. Data is displayed on an LCD screen as traces to allow the operator to monitor the integrity of the system. The data type and sampling interval as provided in Table 4.

Table 4: Acquisition Sampling Rates

Data Type	Sampling
TDEM	0.1 sec
Magnetometer	0.1 sec
GPS Position	0.1 sec
Radar Altimeter	0.2 sec
Laser Altimeter	0.2 sec
Inclinometer	0.2 sec

2.5 BASE STATION

A combined magnetometer/GPS base station was utilized on this project. A Geometrics Caesium vapour magnetometer was used as a magnetic sensor with a sensitivity of 0.001 nT. The base station was recording the magnetic field together with the GPS time at 1 Hz on a base station computer.

The base station magnetometer sensor was installed at the Jamestown Airport (46°55.5' N, 98°40.9' W); away from electric transmission lines and moving ferrous objects such as motor vehicles. The base station data were backed-up to the data processing computer at the end of each survey day.

3. PERSONNEL

The following Geotech Ltd. personnel were involved in the project.

FIELD:

Project Manager:	Darren Tuck (Office)
Data QC:	Neil Fiset (Office)
Crew chief:	Gavin Boege
Operator:	Scott Taylor

The survey pilot and the mechanical engineer were employed directly by the helicopter operator – Geotech Aviation.

Pilot:	Robert Girard
	Paul Winiecki
Mechanical Engineer:	Christine McArthur

OFFICE:

Preliminary Data Processing:	Neil Fiset
Final Data Processing:	Zihao Han
Final Data QA/QC:	Geoffrey Plastow
Final Data Modeling:	Timothy Eadie
Reporting/Mapping:	Wendy Acorn

Processing phase were carried out under the supervision of Data Processing Manager Geoffrey Plastow, P. Geo, and Interpretation phase under the supervision of Director of Geophysics Alexander Prikhodko, P. Geo. The customer relations were looked after by Mandy Long.

4. DATA PROCESSING AND PRESENTATION

Data compilation and processing were carried out by the application of Geosoft OASIS Montaj and programs proprietary to Geotech Ltd.

4.1 FLIGHT PATH

The flight path, recorded by the acquisition program as WGS 84 latitude/longitude, was converted into the WGS84 Datum, UTM Zone 16 North coordinate system in Oasis Montaj.

Both sets of GPS coordinate, from helicopter GPS and magnetic gradiometer GPS, were sampled every 0.1 seconds. A GPS base station, located at the locations listed in Section 2.5 was used in the Differential GPS (DGPS) post-processing of both sets of GPS coordinates. The confidence level of the post-processed DGPS coordinates is excellent for both the helicopter and gradiometer loop GPS based off mean HDOP of 0.91 and 0.92 and PDOP of 1.66 and 1.62, respectively.

The final set of coordinates were then calculated for the position halfway between the two magnetometers that are located on the left and right hand sides of the magnetic gradiometer loop. This position represents the centre of the magnetic gradiomter loop and is the point where the tow cable intersects the plane of the magnetic gradiometer loop. This was achieved by projecting backwards along the flight line by 6.25 m, the radius of the gradiometer loop, from the gradiometer loop GPS antenna position. The EM and magnetic data have been parallax corrected to this set of coordinates and to which all EM and magnetic data and interpretations should be referred.

4.2 CALCULATION OF EM TRANSMITTER RECEIVER LOOP HEIGHT

The EM transmitter-receiver loop height above ground was calculated using the differentially corrected gradiometer loop GPS and derived DEM data. The derived DEM was calculated using the helicopter GPS elevation and radar altimeter measurements, factoring in the vertical separation between the two sensors on the helicopter. This calculated DEM was then corrected to the National Elevation Dataset (NED) over the survey block by removing any linear trends between the two DEM values. The correction of the measured DEM to NED removes first-order errors that could have resulted from the radar altimeter measurement or variations in the quality of the GPS elevation measurements. The EM transmitter-receiver loop height above ground was calculated from the difference between this corrected DEM and the centre of the gradiometer loop elevation accounting for the vertical separation between the gradiometer and EM transmitter-receiver loop using a constant value of 9 metres.

4.3 ELECTROMAGNETIC DATA

As the data are acquired by the data acquisition system on the helicopter, it goes through a digital filter to reject major sferic events and is stacked to further reduce system noise. Afterward, the streamed data is processed by applying a system response correction, B-field integration, time window binning, compensation, filtering, and leveling. Three stages of processing of the EM data have been delivered. They are denoted in the final point-located EM dataset (Table 5) as;

1. Raw (Raw),
2. Filtered (Filt)
3. Final (F).

The digital filtering process is a three stage filter used to reject major sferic events and reduce system noise. Local sferic activity can produce sharp, large amplitude events that cannot be removed by conventional filtering procedures. Smoothing or stacking will reduce their amplitude but leave a broader residual response that can be confused with geological phenomena. To avoid this possibility, a computer algorithm searches out and rejects the major sferic events. The data was then stacked using 15 half cycles, 0.3 seconds, to create a stacked half-cycle waveform at 0.1 second intervals. The stacking coefficients are tapered with a shape that approximates a Gaussian function.

During post-flight processing, the streamed data have a sensor response correction applied which corrects the receiver channels and current monitor to a common impulse response based on the Full Waveform calibration (see Section 2.4.3). The B-field data are calculated by integrating the dB/dt cycles from the 192 kHz streamed data. Then, the streamed data are converted into a set of time window channels (see Table 3) to reduce noise levels further. The output of this stage is the data denoted as "Raw" in Table 5.

The data have noise levels reduced further by the use of an EM compensation procedure which removes characteristic noise from each fiducial determined by the difference between the transmitter and bucking loop fields at the receiver during the flight. This is achieved by a statistical correlation between each time window channel and primary field measurement taken during the on-time. Next, filtering of the electromagnetic data was performed in two steps. The first is a 5 fiducial wide non-linear filter to eliminate any large spikes remaining in the dataset. The second filter is a low pass symmetric linear digital filter that has zero-phase shift which prevents any lag or peak displacement from occurring, and it suppresses only variations with a wavelength less than about 1.5 second or around 40 metres. The data channels which have been processed to this point are denoted by "Filtered" in Table 5.

A "zero level" estimate was subtracted from the data at each fiducial to remove the remaining system response from the data. The "zero level" correction applied was calculated by linear interpolation of the high altitude backgrounds recorded two or more times during each survey flight. Afterwards, a parallax correction was applied to the EM data to account for the distance by which the EM transmitter-receiver loop lags behind the centre of the magnetic gradiometer loop. In this parallax correction the EM data are shuffled toward lower fiducial numbers by the nearest integer number of fiducials that it would take to travel the average horizontal distance which separates the centres of the magnetic gradiometer and EM loops based on the average helicopter speed for each line. This produces the EM data denoted as "Final" in Table 5.

VTEM™ has three receiver coil orientations. Z-axis coil is oriented parallel to the transmitter coil axis and both are horizontal to the ground. The X-axis coil is oriented parallel to the ground and along the line-of-flight. The Y-axis coil is oriented parallel to the ground and perpendicular to the line-of-flight. This combined three coil configuration provides information on the position, depth, dip and thickness of a conductor. Generalized modeling results of VTEM data, are shown in Appendix D.

In general X-component data produce cross-over type anomalies: from "+ to – "in flight direction of flight for "thin" sub vertical targets and from "- to +" in direction of flight for "thick" targets. Z component data produce double peak type anomalies for "thin" sub vertical targets and single peak for "thick" targets.

4.4 HORIZONTAL MAGNETIC GRADIOMETER DATA

The horizontal gradients data from the VTEM™Plus are measured by two magnetometers 12.5 m apart on an independent bird mounted 9m above the VTEM™ loop. A GPS and a Gyro Inclinometer help to determine the positions and orientations of the magnetometers. The data from the two magnetometers are corrected for position and orientation variations, as well as for the diurnal variations using the base station data.

The position of the centre of the horizontal magnetic gradiometer bird is calculated form the GPS utilizing in-house processing tool in Geosoft. Following that total magnetic intensity is calculated at the center of the bird by calculating the mean values from both sensors. In addition to the total intensity advanced processing is done to calculate the in-line and cross-line (or lateral) horizontal gradient which enhance the understanding of magnetic targets. The in-line (longitudinal) horizontal gradient is calculated from the difference of two consecutive total magnetic field readings divided by the distance along the flight line direction, while the cross-line (lateral) horizontal magnetic gradient is calculated from the difference in the magnetic readings from both magnetic sensors divided by their horizontal separation.

Two advanced magnetic derivative products, the total horizontal derivative (THDR), and tilt angle derivative and are also created. The total horizontal derivative or gradient is defined as:

THDR = sqrt(Hx*Hx+Hy*Hy), where Hx and Hy are cross-line and in-line horizontal gradients.

The tilt angle derivative (TDR) is defined as:

TDR = arctan(Vz/THDR), where THDR is the total horizontal derivative, and Vz is the vertical derivative.

Measured cross-line gradients can help to enhance cross-line linear features during gridding.

5. 1D INVERSION MODELS

The final processed data was used as the input modeling over the entire block. The algorithm used for the inversion modeling was GALEISBSTDEM[3] which is a one dimensional (1D) layered earth deterministic algorithm designed to invert airborne time-domain electromagnetic data. Since the algorithm is 1D, it assumes that the Earth is horizontally stratified and laterally-uniform layer conductivities and thicknesses. For VTEM, the 1D assumption works well in a stratified geology due to the limited lateral sensitivity of the system's measurement outside of its footprint[4]. Each of these 1D inversion models can be "stitched" together to form visualizations of the layer conductivities along the flight line in 2D and for the entire block in 3D.

The GALEISBSTDEM algorithm has two modeling options: a multi-layer smooth model which solves for the layer's conductivity while the thicknesses remain fixed, or a few-layer blocky model which solves for both the layer's conductivity and thickness. Since the inversion problem for AEM is under-determined, the solution is non-unique and regularization is needed to constrain the model results. The multi-layer smooth model constrains the inversion by fitting only smoothly varying conductivity models with respect to depth which acts as a way to regularize the results. The main constraint for a few-layer blocky model is the number of initial layers in the reference model since this option attempts to resolve a model that reflects the conductivity and thickness of each geological layer. The multi-layer smooth model option works best when there is little prior information about the expected model results due to the smooth nature of the regularization. However, this option is not able to accurately define individual geological layer thicknesses, conductivities, or depths to geological boundaries. To resolve those more accurately, the few-layer blocky model option is necessary but requires accurate estimations of the starting models number of layers and conductivity. The blocky model option has the ability to apply probabilistic constraints to each of the conductivity and thickness values in the starting model. These constraints restrict or penalize the inversion algorithm from deviating from the starting model values. Therefore, this additional method of constraining the inversion can be use when there is prior information about the geology, like well logs or boreholes.

For this survey, the inversion process began by using the multi-layer smooth option to model the final processed data. The starting model consisted of 25 layers with a starting thickness of 2.5 metres and grew logarithmically to a depth of 250 metres plus a basement layer. Each of these layers started from resistivity of 33 ohm-m. This inversion and each subsequent inversion run inverted every 5th sounding which results in a separation of 12-15 metres for each inverted model. Testing was conducted which showed that this data decimation did not impact the model resolution. The inversion was able to fit these models within the misfit for each of the soundings not heavily influence by cultural noise. The inversion model results were able to show the general structure of the geology's conductivity profile. The models show a variably conductive layer at surface typically between 10-30 ohm-m. The top of the aquifer begins to show around 50-60 metres in depth with a very conductive layer below the aquifer which coincides with the Pierre Shale formation from the well logs.

---

[3] https://github.com/GeoscienceAustralia/ga-aem
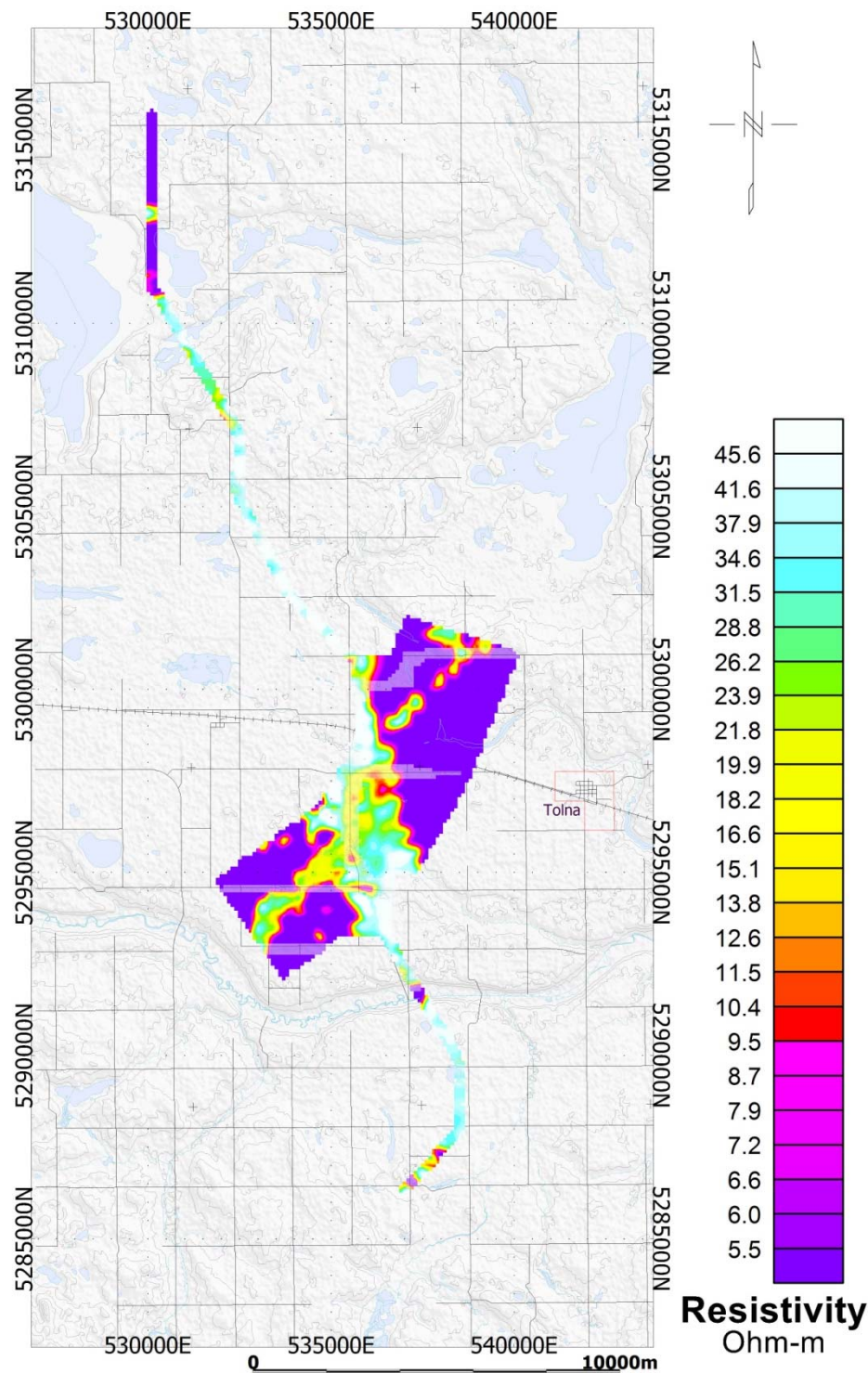[4] Reid et al. 2006, Airborne electromagnetic footprints in 1D earths: Geophysics, 71, no. 2, pG63-G72.

Figure 6: Resistivity Depth Slice at 80 m from 1D blocky constrained inversion models.

In order to create models which were more representative to the geology, the final data was next inverted using the few-layer blocky option. The number of layers for the starting model was derived from analysis of the smooth models and geological structure of the nearby Spiritwood-JT inversion

results. The number of layers selected for the starting model was 10, 9 layers where the inversion solved for the conductivity and thickness plus a basement layer. The results from these inversions showed similar structure as the smooth inversion models but better definition of each geological layer's conductivity and thickness. Although the models fit the data well, when they were compared against the measured well log resistivity profiles, there were some discrepancies in the first few layer. The block models tended to resolve the first layers as more resistive and conductive, respectively, than the well log measurements due to having too much freedom during the modeling process. Therefore, a third set of inversion models were calculated by applying probabilistic constraints to the near-surface layer's conductivity and thickness values. These blocky constrained models both fit the data and more closely resembled the well log resistivity profiles in the top tens of metres.

The final blocky constrained models were effective at mapping the Spiritwood-Warwick aquifer in three dimensions. The inversion results show the top of the aquifer to start around 50 metres in depth across the main block portion of the survey. Deeper at 80 metres shown in Figure 6, the results show two main resistive features within the survey block with most likely coincide with the central channels of aquifers which have cut into the underlying shale. The larger of the two is a north-south trending aquifer and crosses through the middle of the survey block. This same feature can be seen along the regional lines (L1300-L1380) to the north and south of the block. This feature appears to be the Spiritwood-Warwick aquifer as its location and trajectory match what has previously been mapped. The second feature crosses through the block in a northeast-southwest direction and intersects with Spiritwood in the middle of the block. This channel aquifer is thinner at its northeast portion, around 25-30 metres thick, and thickens as it moves southwest to around 75 metres in thickness. Based on the elevations of the aquifer at each end of the survey block, it appears to flow towards the southwest. This can be seen in the two cross-section resistivity models of lines 1050 and 1280 presented in Figure 7 with the aquifer located at 537400E on L1050 and 5293200N on L1280.
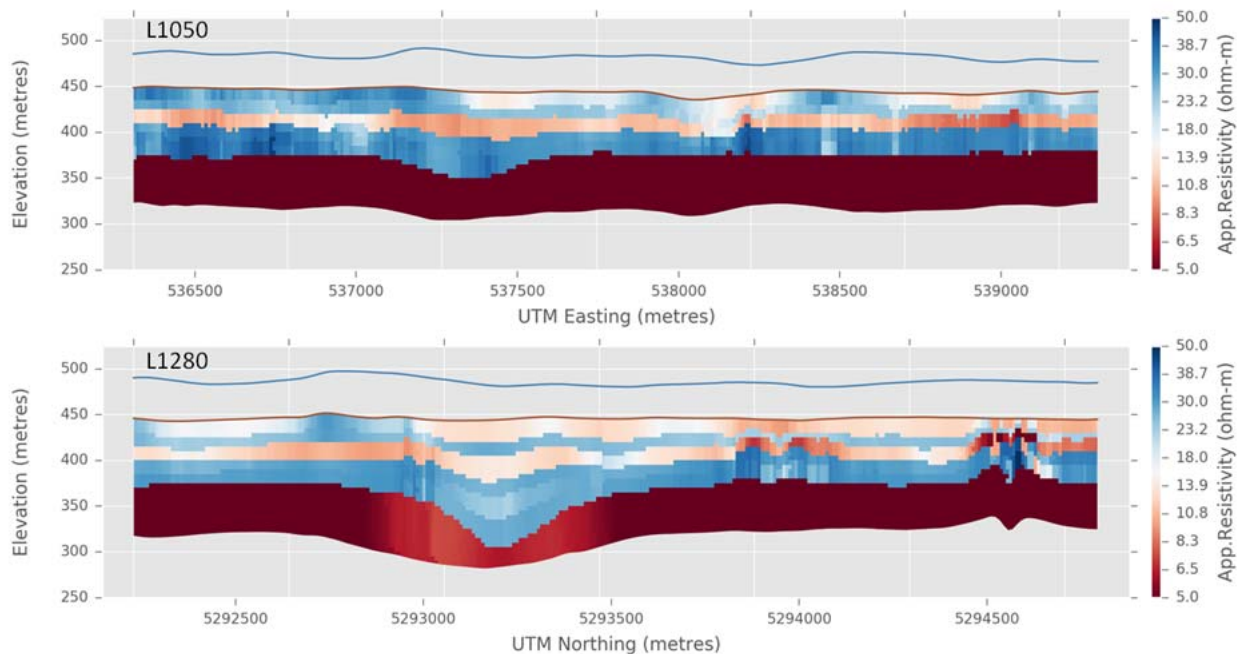
Figure 7: Resistivity cross-section of 1D blocky constrained inversion models for L1050 (top) and L1280 (bottom).

From the final blocky constrained models, several products were generated which visualize the resistivity models in different perspectives. The products include: planar resistivity depth slices at 10 metre intervals, cross-sectional resistivity model for each flight line and tie line, and a 3D gridded voxel composed from each of the 1D resistivity inversion models which provides a 3D perspective of the resistivity variation across the entire survey block.

6. DELIVERABLES

6.1 SURVEY REPORT

The survey report describes the data acquisition, processing, 1D inversion modeling, and final presentation of the survey results. The survey report is provided in two paper copies and digitally in PDF format.

6.2 MAPS

Final maps were produced at scale of 1:50,000 for best representation of the survey size and line spacing. The coordinate/projection system used was WGS84 Datum, UTM Zone 14 North. All maps show the flight path trace and topographic data; latitude and longitude are also noted on maps.

The preliminary and final results of the survey are presented as EM profiles, a late-time gate gridded EM channel, and a colour magnetic TMI contour map.

- Maps at 1:50,000 in Geosoft MAP format, as follows:

    GL160299_50k_dBdt: dB/dt profiles Z Component, Time Gates 0.220 – 7.036 ms in linear – logarithmic scale.
    GL160299_50k_Bfield: B-field profiles Z Component, Time Gates 0.220 – 7.036 ms in linear – logarithmic scale.
    GL160299_50k_BFz36:   B-field time Z Component Channel 36, Time Gate 2.021 ms colour image.
    GL160299_50k_TMI: Total magnetic intensity (TMI) colour image and contours.
    GL160299_50k_TotHGrad: Magnetic Total Horizontal Gradient colour image.
    GL160299_50k_TiltDrv: Magnetic Tilt-Angle Derivative colour image.

- Maps are also presented in PDF format.
- The topographic data base was derived from ND State Water Commission Data Portal www.mapservice.swc.nd.gov and Geocommunities www.geocomm.com.
- A Google Earth file *GL160299_NDakota.kml* showing the flight path of the block is included. Free versions of Google Earth software from: http://earth.google.com/download-earth.html

6.3 DIGITAL DATA

Two copies of the data on DVD were prepared to accompany the report. Each DVD contains a digital file of the line data in GDB Geosoft Montaj format.

- DVD structure.

    Data   contains databases, grids and maps, as described below.
    Report   contains a copy of the report and appendices in PDF format.

Databases in Geosoft GDB format, containing the channels listed in Table 5.

Table 5: Geosoft GDB Data Format

Channel name	Units	Description
X:	metres	UTM Easting WGS84 Zone 14 North
Y:	metres	UTM Northing WGS84 Zone 14 North
Longitude:	Decimal Degrees	WGS 84 Longitude data
Latitude:	Decimal Degrees	WGS 84 Latitude data
Z:	metres	GPS antenna elevation
Zb:	metres	EM bird elevation
Radar:	metres	helicopter terrain clearance from radar altimeter
Radarb:	metres	Calculated EM transmitter-receiver loop terrain clearance from radar altimeter and two GPS elevations
DEM:	metres	Digital Elevation Model
Gtime:	Seconds of the day	GPS time
Laser	meters	Gradiometer Loop laser altimeter height above ground
Mag1L:	nT	Measured Total Magnetic field data (left sensor)
Mag1R:	nT	Measured Total Magnetic field data (right sensor)
Basemag:	nT	Magnetic diurnal variation data
Mag2LZ	nT	Z corrected (w.r.t. loop center) and diurnal corrected magnetic field left mag
Mag2RZ	nT	Z corrected (w.r.t. loop center) and diurnal corrected magnetic field right mag
TMI2	nT	Calculated from diurnal corrected total magnetic field intensity of the centre of the loop
TMI3	nT	Microleveled total magnetic field intensity of the centre of the loop
Hginline		Calculated in-line gradient
Hgcxline		measured cross-line gradient
CVG	nT/m	Calculated Magnetic Vertical Gradient
PLM:		60 Hz power line monitor
SFz[4]:	$pV/(A*m4)$	Final Z dB/dt 0.021 millisecond time channel
SFz[5]:	$pV/(A*m4)$	Final Z dB/dt 0.026 millisecond time channel
SFz[6]:	$pV/(A*m^4)$	Final Z dB/dt 0.031 millisecond time channel
SFz[7]:	$pV/(A*m^4)$	Final Z dB/dt 0.036 millisecond time channel
SFz[8]:	$pV/(A*m^4)$	Final Z dB/dt 0.042 millisecond time channel
SFz[9]:	$pV/(A*m^4)$	Final Z dB/dt 0.048 millisecond time channel
SFz[10]:	$pV/(A*m^4)$	Final Z dB/dt 0.055 millisecond time channel
SFz[11]:	$pV/(A*m^4)$	Final Z dB/dt 0.063 millisecond time channel
SFz[12]:	$pV/(A*m^4)$	Final Z dB/dt 0.073 millisecond time channel
SFz[13]:	$pV/(A*m^4)$	Final Z dB/dt 0.083 millisecond time channel
SFz[14]:	$pV/(A*m^4)$	Final Z dB/dt 0.096 millisecond time channel
SFz[15]:	$pV/(A*m^4)$	Final Z dB/dt 0.110 millisecond time channel
SFz[16]:	$pV/(A*m^4)$	Final Z dB/dt 0.126 millisecond time channel
SFz[17]:	$pV/(A*m^4)$	Final Z dB/dt 0.145 millisecond time channel
SFz[18]:	$pV/(A*m^4)$	Final Z dB/dt 0.167 millisecond time channel
SFz[19]:	$pV/(A*m^4)$	Final Z dB/dt 0.192 millisecond time channel
SFz[20]:	$pV/(A*m^4)$	Final Z dB/dt 0.220 millisecond time channel
SFz[21]:	$pV/(A*m^4)$	Final Z dB/dt 0.253 millisecond time channel
SFz[22]:	$pV/(A*m^4)$	Final Z dB/dt 0.290 millisecond time channel
SFz[23]:	$pV/(A*m^4)$	Final Z dB/dt 0.333 millisecond time channel

Channel name	Units	Description
SFz[24]:	pV/(A*m^4)	Final Z dB/dt 0.383 millisecond time channel
SFz[25]:	pV/(A*m^4)	Final Z dB/dt 0.440 millisecond time channel
SFz[26]:	pV/(A*m^4)	Final Z dB/dt 0.505 millisecond time channel
SFz[27]:	pV/(A*m^4)	Final Z dB/dt 0.580 millisecond time channel
SFz[28]:	pV/(A*m^4)	Final Z dB/dt 0.667 millisecond time channel
SFz[29]:	pV/(A*m^4)	Final Z dB/dt 0.766 millisecond time channel
SFz[30]:	pV/(A*m^4)	Final Z dB/dt 0.880 millisecond time channel
SFz[31]:	pV/(A*m^4)	Final Z dB/dt 1.010 millisecond time channel
SFz[32]:	pV/(A*m^4)	Final Z dB/dt 1.161 millisecond time channel
SFz[33]:	pV/(A*m^4)	Final Z dB/dt 1.333 millisecond time channel
SFz[34]:	pV/(A*m^4)	Final Z dB/dt 1.531 millisecond time channel
SFz[35]:	pV/(A*m^4)	Final Z dB/dt 1.760 millisecond time channel
SFz[36]:	pV/(A*m^4)	Final Z dB/dt 2.021 millisecond time channel
SFz[37]:	pV/(A*m^4)	Final Z dB/dt 2.323 millisecond time channel
SFz[38]:	pV/(A*m^4)	Final Z dB/dt 2.667 millisecond time channel
SFz[39]:	pV/(A*m^4)	Final Z dB/dt 3.063 millisecond time channel
SFz[40]:	pV/(A*m^4)	Final Z dB/dt 3.521 millisecond time channel
SFz[41]:	pV/(A*m^4)	Final Z dB/dt 4.042 millisecond time channel
SFz[42]:	pV/(A*m^4)	Final Z dB/dt 4.641 millisecond time channel
SFz[43]:	pV/(A*m^4)	Final Z dB/dt 5.333 millisecond time channel
SFz[44]:	pV/(A*m^4)	Final Z dB/dt 6.125 millisecond time channel
SFz[45]:	pV/(A*m^4)	Final Z dB/dt 7.036 millisecond time channel
SFz[46]:	pV/(A*m^4)	Final Z dB/dt 8.083 millisecond time channel
SFx[20]:	pV/(A*m^4)	Final X dB/dt 0.220 millisecond time channel
SFx[21]:	pV/(A*m^4)	Final X dB/dt 0.253 millisecond time channel
SFx[22]:	pV/(A*m^4)	Final X dB/dt 0.290 millisecond time channel
SFx[23]:	pV/(A*m^4)	Final X dB/dt 0.333 millisecond time channel
SFx[24]:	pV/(A*m^4)	Final X dB/dt 0.383 millisecond time channel
SFx[25]:	pV/(A*m^4)	Final X dB/dt 0.440 millisecond time channel
SFx[26]:	pV/(A*m^4)	Final X dB/dt 0.505 millisecond time channel
SFx[27]:	pV/(A*m^4)	Final X dB/dt 0.580 millisecond time channel
SFx[28]:	pV/(A*m^4)	Final X dB/dt 0.667 millisecond time channel
SFx[29]:	pV/(A*m^4)	Final X dB/dt 0.766 millisecond time channel
SFx[30]:	pV/(A*m^4)	Final X dB/dt 0.880 millisecond time channel
SFx[31]:	pV/(A*m^4)	Final X dB/dt 1.010 millisecond time channel
SFx[32]:	pV/(A*m^4)	Final X dB/dt 1.161 millisecond time channel
SFx[33]:	pV/(A*m^4)	Final X dB/dt 1.333 millisecond time channel
SFx[34]:	pV/(A*m^4)	Final X dB/dt 1.531 millisecond time channel
SFx[35]:	pV/(A*m^4)	Final X dB/dt 1.760 millisecond time channel
SFx[36]:	pV/(A*m^4)	Final X dB/dt 2.021 millisecond time channel
SFx[37]:	pV/(A*m^4)	Final X dB/dt 2.323 millisecond time channel
SFx[38]:	pV/(A*m^4)	Final X dB/dt 2.667 millisecond time channel
SFx[39]:	pV/(A*m^4)	Final X dB/dt 3.063 millisecond time channel
SFx[40]:	pV/(A*m^4)	Final X dB/dt 3.521 millisecond time channel
SFx[41]:	pV/(A*m^4)	Final X dB/dt 4.042 millisecond time channel
SFx[42]:	pV/(A*m^4)	Final X dB/dt 4.641 millisecond time channel
SFx[43]:	pV/(A*m^4)	Final X dB/dt 5.333 millisecond time channel
SFx[44]:	pV/(A*m^4)	Final X dB/dt 6.125 millisecond time channel
SFx[45]:	pV/(A*m^4)	Final X dB/dt 7.036 millisecond time channel
SFx[46]:	pV/(A*m^4)	Final X dB/dt 8.083 millisecond time channel

Channel name	Units	Description
SFx	pV/(A*m^4)	Final Y dB/dt data for time channels 20 to 46
BFz	(pV*ms)/(A*m^4)	Final Z B-Field data for time channels 4 to 46
BFx	(pV*ms)/(A*m^4)	Final X B-Field data for time channels 20 to 46
BFy	(pV*ms)/(A*m^4)	Final Y B-Field data for time channels 20 to 46
SFxFF	pV/(A*m^4)	Fraser Filtered X dB/dt
SRawz	pV/(A*m^4)	Raw Z dB/dt data for time channels 4 to 46
SRawx	pV/(A*m^4)	Raw X dB/dt data for time channels 20 to 46
SRawy	pV/(A*m^4)	Raw Y dB/dt data for time channels 20 to 46
BRawz	(pV*ms)/(A*m^4)	Raw Z B-Field data for time channels 4 to 46
BRawx	(pV*ms)/(A*m^4)	Raw X B-Field data for time channels 20 to 46
BRawy	(pV*ms)/(A*m^4)	Raw Y B-Field data for time channels 20 to 46
SFltz	pV/(A*m^4)	Filtered Z dB/dt data for time channels 4 to 46
SFltx	pV/(A*m^4)	Filtered X dB/dt data for time channels 20 to 46
SFlty	pV/(A*m^4)	Filtered Y dB/dt data for time channels 20 to 46
BFltz	(pV*ms)/(A*m^4)	Filtered Z B-Field data for time channels 4 to 46
BFltx	(pV*ms)/(A*m^4)	Filtered X B-Field data for time channels 20 to 46
BFlty	(pV*ms)/(A*m^4)	Filtered Y B-Field data for time channels 20 to 46

Electromagnetic B-field and dB/dt Z component data is found in array channel format between indexes 4 – 46, X component data from 20 – 46, and Y component data from 20 – 46, as described above.

- Database of the VTEM Waveform "GL160299_waveform_final.gdb" in Geosoft GDB format, containing the following channels:

Table 6: Geosoft database for the VTEM waveform

Channel name	Units	Description
Time:	milliseconds	Sampling rate interval, 5.2083 microseconds
Tx_Current:	amps	Output current of the transmitter

- EM and Magnetic Data Grids in Geosoft GRD and GFX format, as follows:

BFz36:	B-Field Z Component Channel 36 (Time Gate 2.021 ms)
DEM:	Digital Elevation Model (metres)
CVG:	Calculated Vertical Derivative (nT/m)
PLM:	Power Line Monitor (60 Hz)
Hgcxline:	Measured Cross-Line Gradient (nT/m)
Hginline:	Measured In-Line Gradient (nT/m)
TMI3:	Total Magnetic Intensity (nT)
TotHgrad:	Magnetic Total Horizontal Gradient (nT/m)
Tiltdrv:	Magnetic Tilt derivative (radians)
SFz4:	dB/dt Z Component Channel 4 (Time Gate 0.021 ms)
SFz20:	dB/dt Z Component Channel 20 (Time Gate 0.220 ms)
SFz40:	dB/dt Z Component Channel 40 (Time Gate 3.521 ms)

A Geosoft .GRD file has a .GI metadata file associated with it, containing grid projection information. A grid cell size of 100 metres was used.

The EM 1D Inversion Models and products have been provided as follows:

- Final Inversion models in space delimited ASCII column data file, DAT format, with accompanied header files
- Planar resistivity depth slice grids at 10 metre intervals in Geosoft GRD and GXF formats
- Cross-section resistivity models for each line and tie line in Geosoft GRD and GXF formats
- 3D gridded resistivity voxel in Geosoft voxel and Geosoft XYZ format

6.4 FLIGHT VIDEO

Video was also recorded during the survey and is included in the final digital data.

7. CONCLUSIONS AND RECOMMENDATIONS

A helicopter-borne versatile time domain electromagnetic (VTEM™plus), horizontal magnetic gradiometer geophysical survey has been completed over the Warwick-Low K Barrier Block situated near Jamestown, North Dakota.
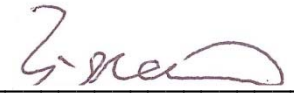
The total area coverage is 36 km². Total survey line coverage 112 line kilometres. The principal sensors included a Time Domain EM system, horizontal magnetic gradiometer using two caesium magnetometers system. Results have been presented as stacked profiles, and contour colour images at a scale of 1:50,000. A formal Interpretation has not been included or requested.
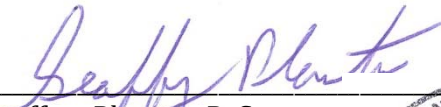
The electromagnetic data collected over the Warwick-Low K Barrier block was of high quality with very strong signal-to-noise ratios. This data was inverted with the 1D GALEISBSTDEM algorithm to produce resistivity models. These models were able to resolve the location and depths to the top and bottom of the Spiritwood-Warwick aquifer throughout the central portion of the block in a north-to-south direction. In addition to resolving the main Spiritwood aquifer, the data and models showed another aquifer which crossed the survey block in a northeast-to-southwest direction and intersected with the Spiritwood-Warwick aquifer in the center of the block. It is unknown if these two aquifers are joined and follow-up drilling at the intersection is recommended.

Based on the model results, it is recommended to drill any areas of interest. The drilling results will provide concrete results about the geology in these areas and information from them could be included in future inversion runs to constrain the models more effectively.
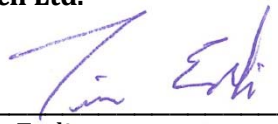
Respectfully submitted[5],

_____
Neil Fiset
Geotech Ltd.

_____
Geoffrey Plastow, P. Geo.
Data Processing Manager
Geotech Ltd.

March, 2017

_____
Zihao Han
Geotech Ltd.

_____
Timothy Eadie
Geotech Ltd.

_____
Alexander Prikhodko, PhD, P.Geo
Director of Geophysics
Geotech Ltd.

---

[5] Final data processing of the EM and magnetic data were carried out by Neil Fiset, Zihao Han and Timothy Eadie from the office of Geotech Ltd. in Aurora, Ontario, under the supervision of Geoffrey Plastow, P.Geo. Data Processing Manager.

APPENDIX A

SURVEY AREA LOCATION MAP
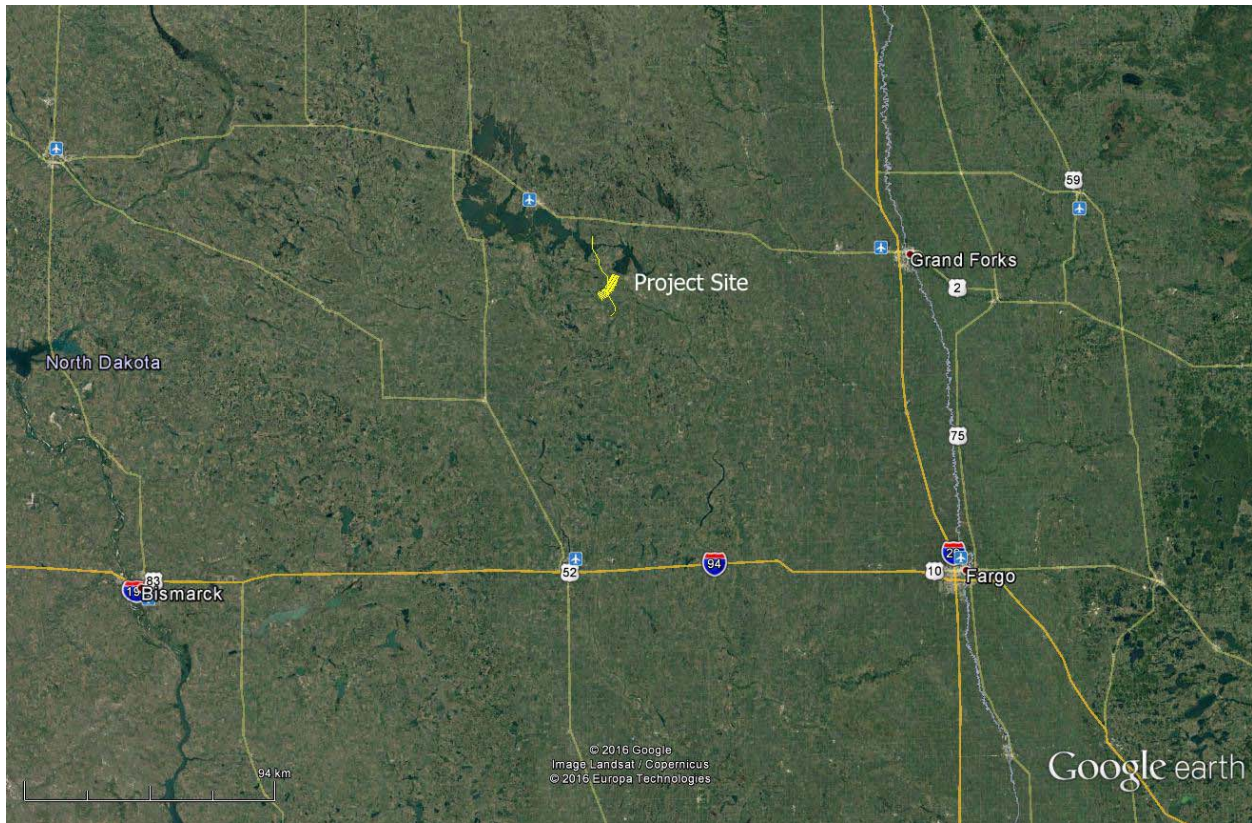
Overview of the Survey Area

APPENDIX B

SURVEY AREA COORDINATES
(WGS 84, UTM Zone 14 North)

Area 1		Area 2	
X	Y	X	Y
537118	5301819	537167	5295011
535683	5298232	535472	5297477
534297	5295884	534784	5296770
537167	5295011	532261	5294931
538553	5297358	533960	5292459
539988	5300945	536483	5294297

APPENDIX C

GEOPHYSICAL MAPS[1]
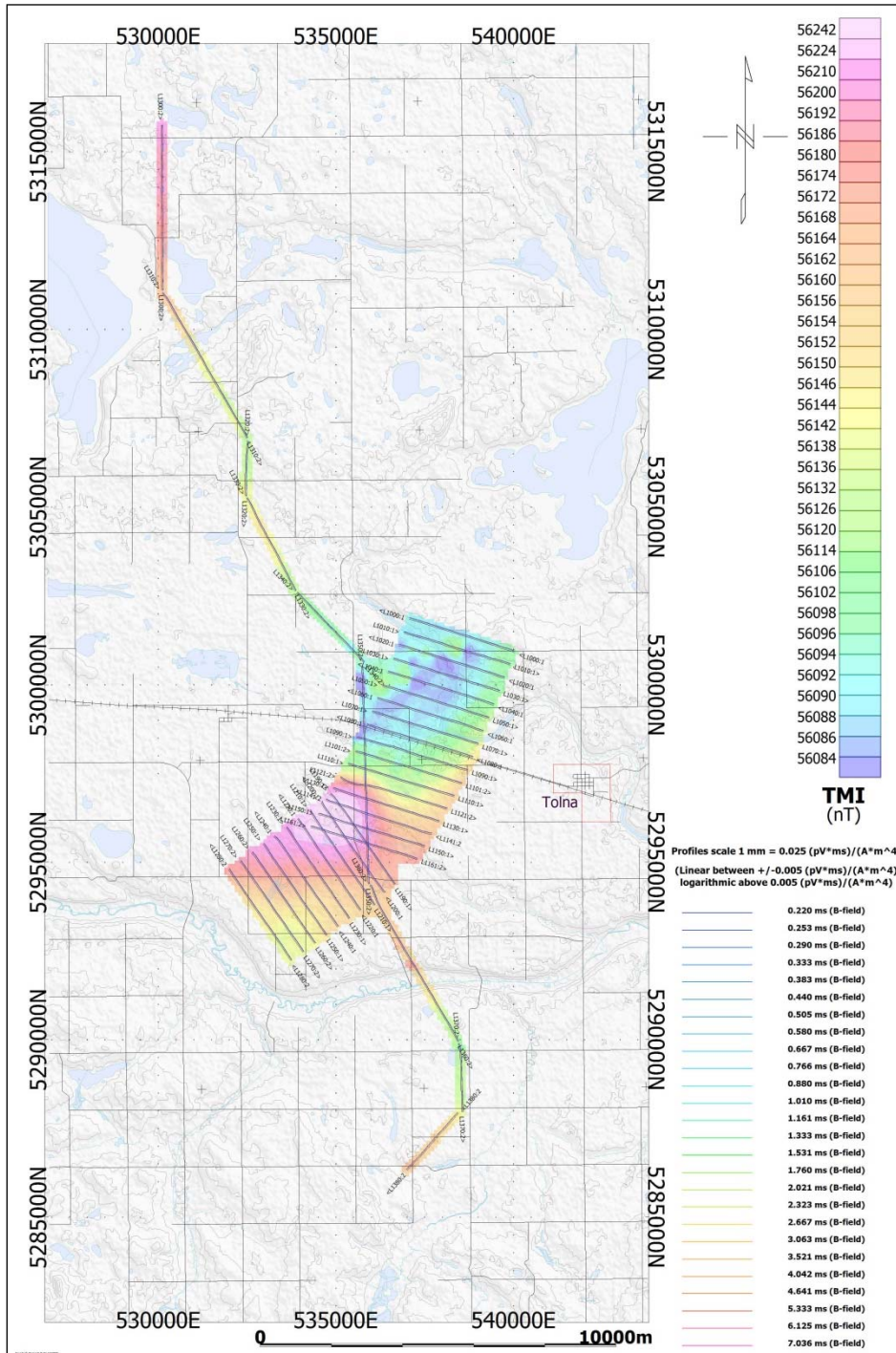
VTEM B-Field Z Component Profiles, Time Gates 0.220 to 7.036 ms

---

[1] Complete full size geophysical maps are also available in PDF format located in the final data maps folder
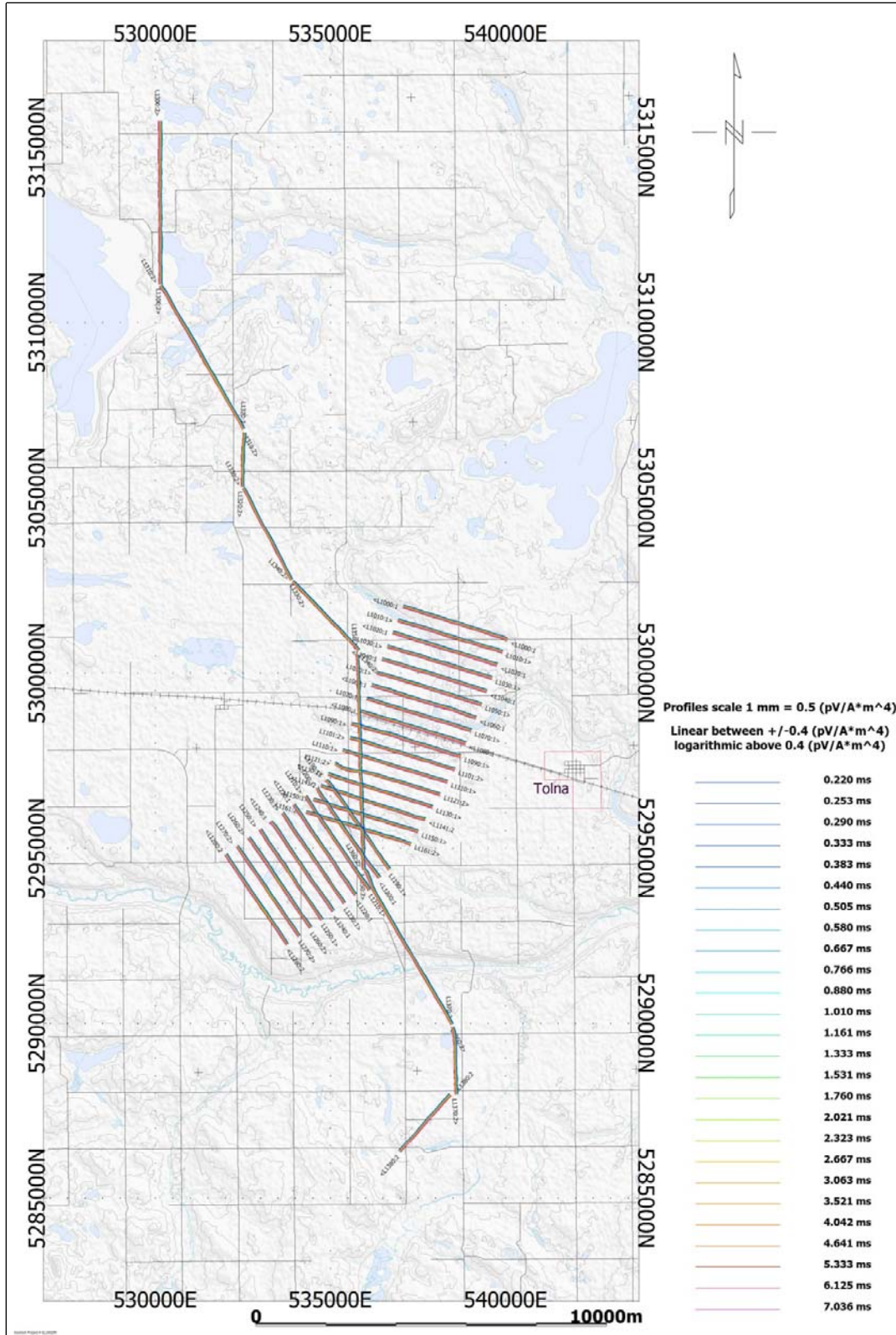
VTEM dB/dt Z Component Profiles, Time Gates 0.220 to 7.036 ms

VTEM B-Field Z Component Channel 36, Time Gate 2.021 ms
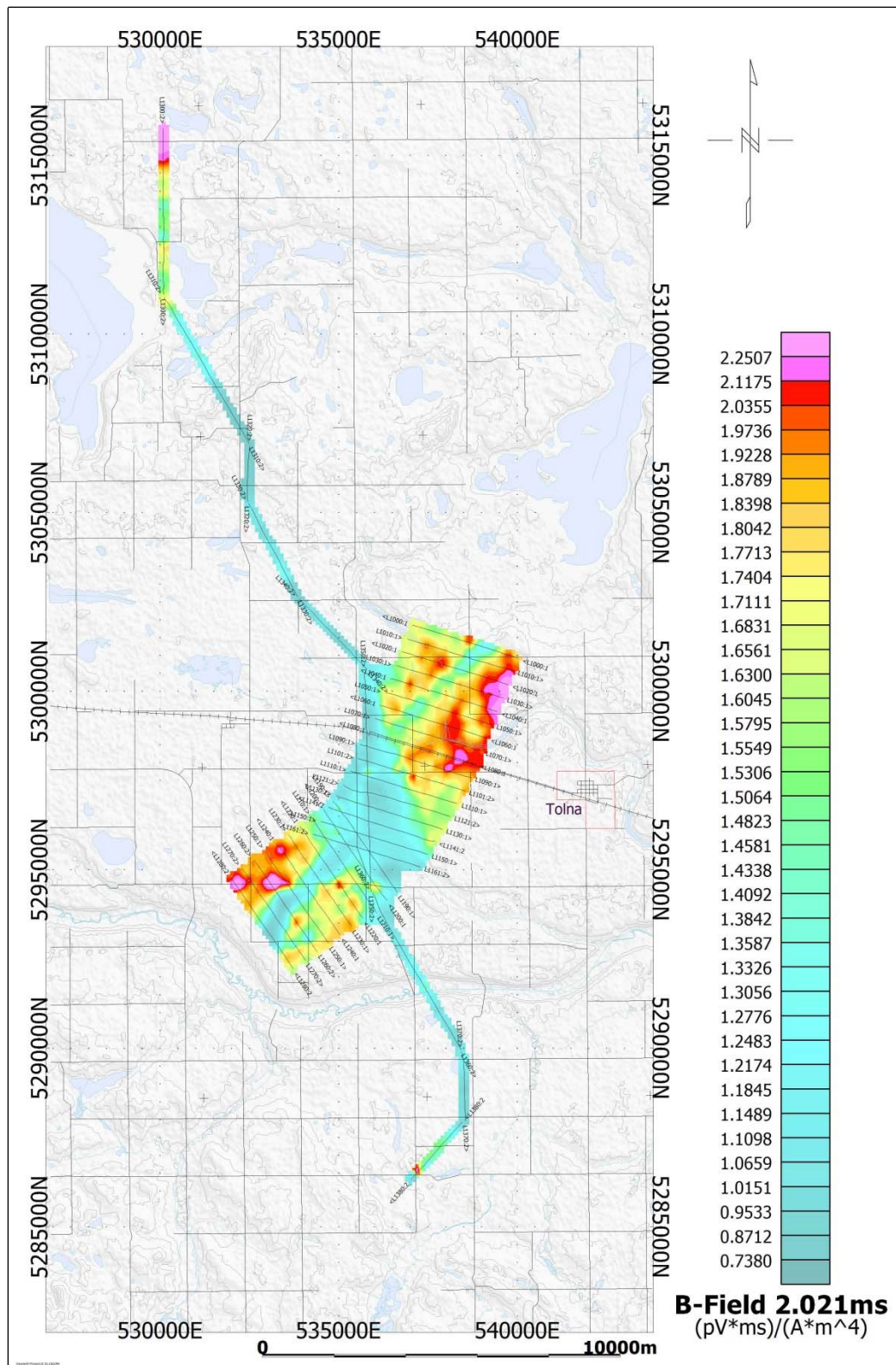
B-Field 2.021ms
(pV*ms)/(A*m^4)

GEOTECH
AIRBORNE GEOPHYSICAL SURVEYS
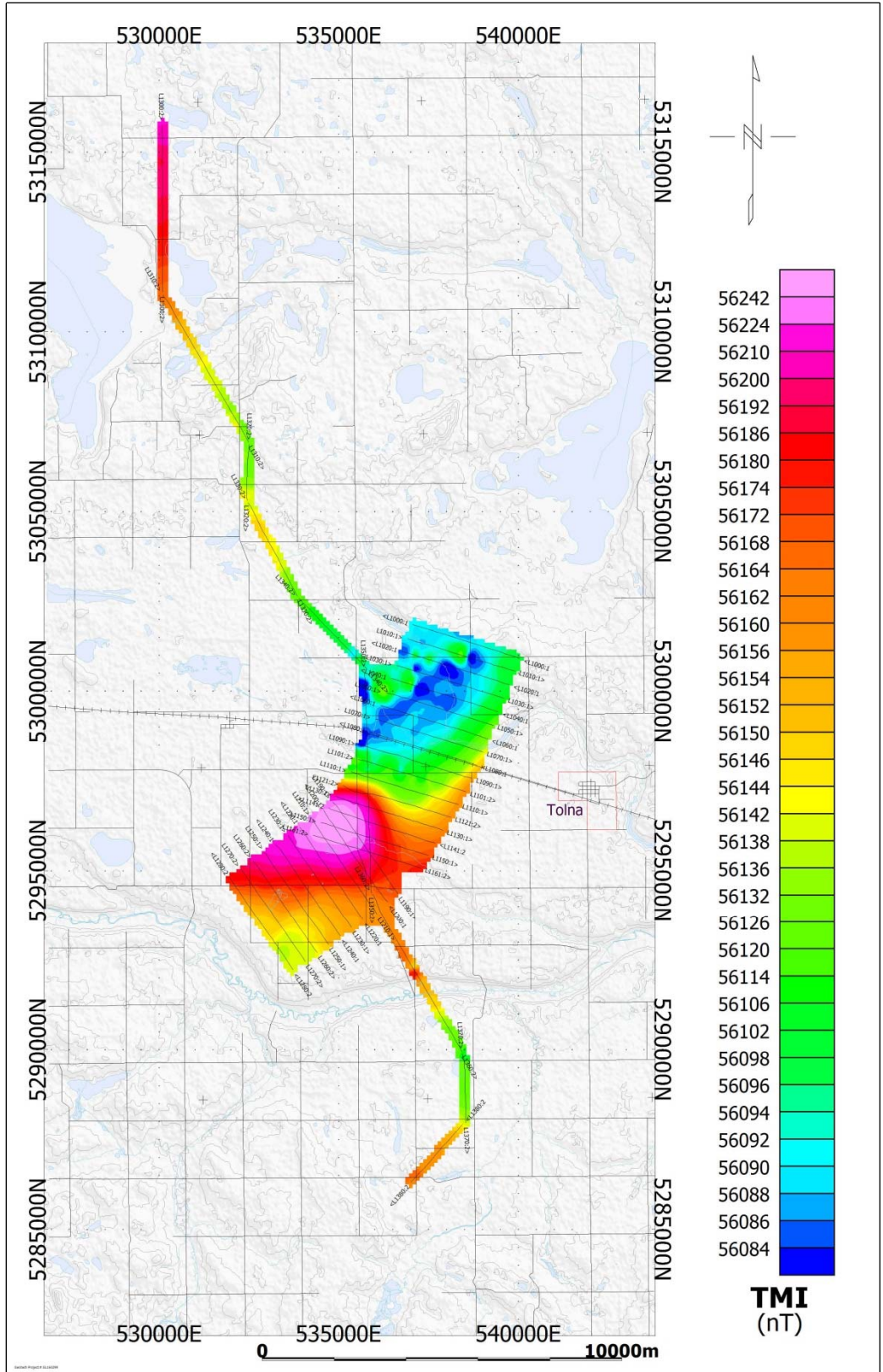
Total Magnetic Intensity (TMI)
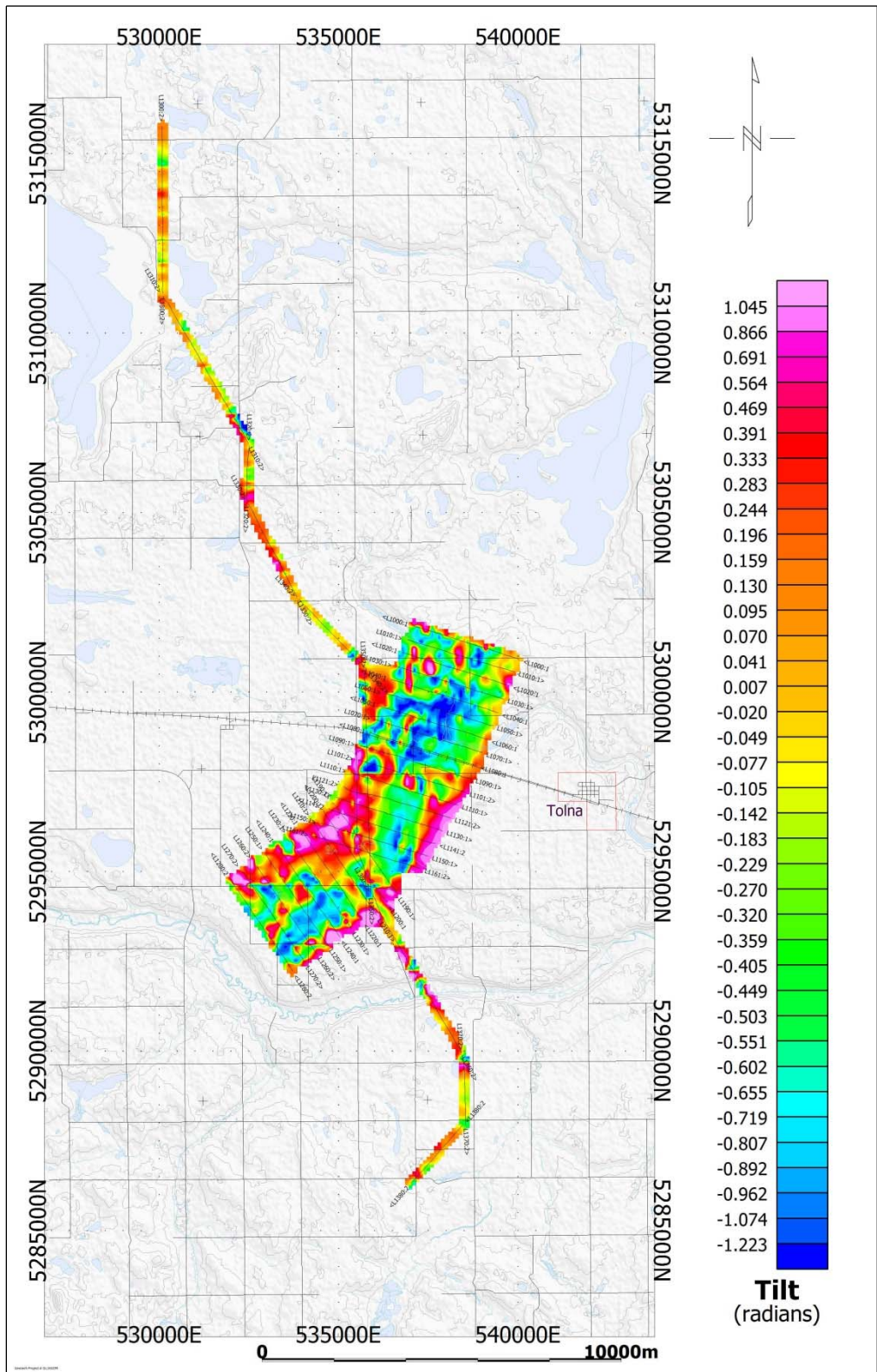
Magnetic Tilt – Angle Derivative
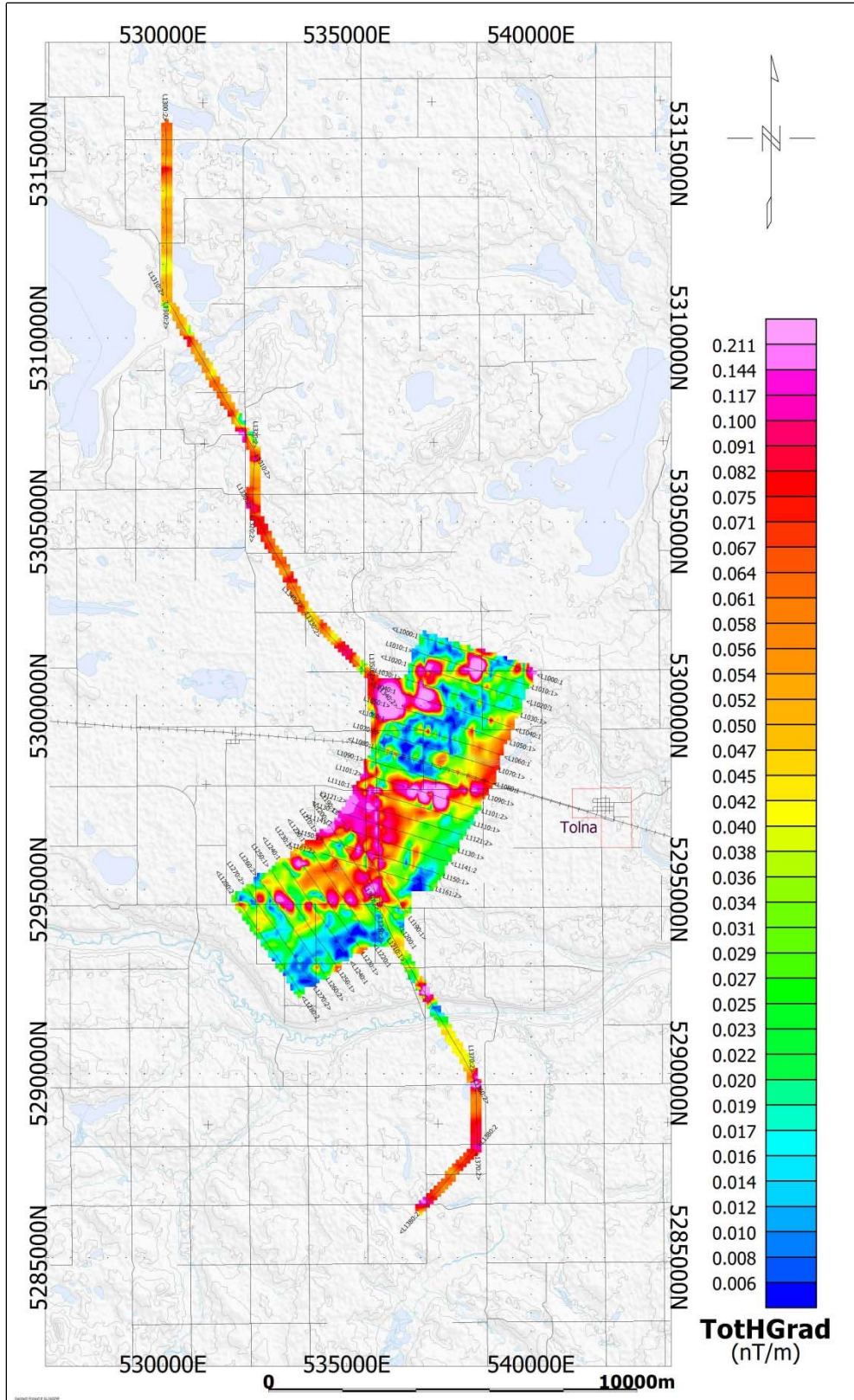
Magnetic Total Horizontal Gradient

APPENDIX D

GENERALIZED MODELING RESULTS OF THE VTEM SYSTEM
INTRODUCTION

The VTEM system is based on a concentric or central loop design, whereby, the receiver is positioned at the centre of a transmitter loop that produces a primary field. The wave form is a bi-polar, modified square wave with a turn-on and turn-off at each end.

During turn-on and turn-off, a time varying field is produced (dB/dt) and an electro-motive force (emf) is created as a finite impulse response. A current ring around the transmitter loop moves outward and downward as time progresses. When conductive rocks and mineralization are encountered, a secondary field is created by mutual induction and measured by the receiver at the centre of the transmitter loop.

Efficient modeling of the results can be carried out on regularly shaped geometries, thus yielding close approximations to the parameters of the measured targets. The following is a description of a series of common models made for the purpose of promoting a general understanding of the measured results.

A set of models has been produced for the Geotech VTEM™ system dB/dT Z and X components (see models D1 to D15). The Maxwell ™ modeling program (EMIT Technology Pty. Ltd. Midland, WA, AU) used to generate the following responses assumes a resistive half-space. The reader is encouraged to review these models, so as to get a general understanding of the responses as they apply to survey results. While these models do not begin to cover all possibilities, they give a general perspective on the simple and most commonly encountered anomalies.

As the plate dips and departs from the vertical position, the peaks become asymmetrical.

As the dip increases, the aspect ratio (Min/Max) decreases and this aspect ratio can be used as an empirical guide to dip angles from near 90º to about 30º. The method is not sensitive enough where dips are less than about 30º.
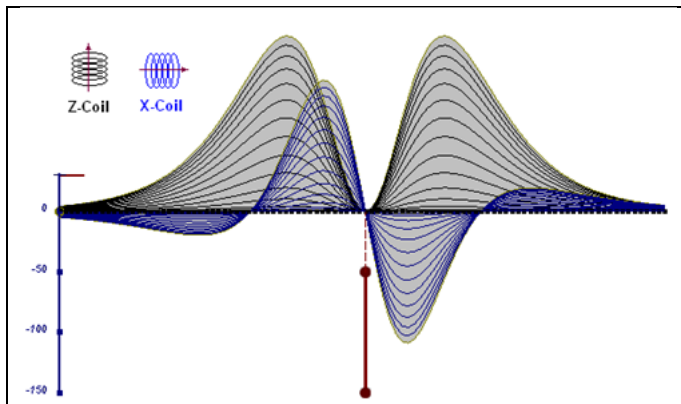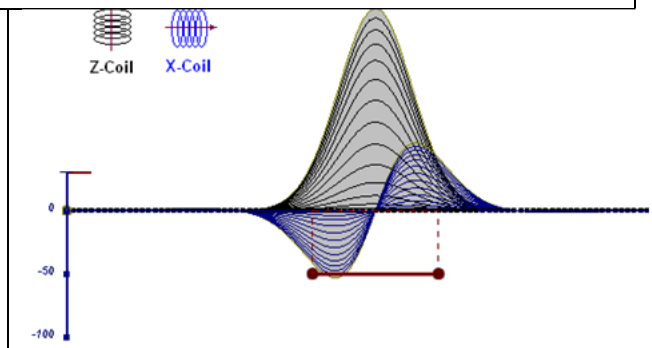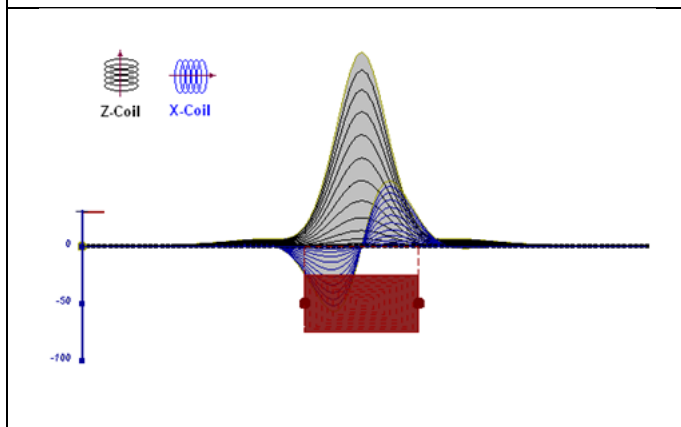
Figure D-1: vertical thin plate
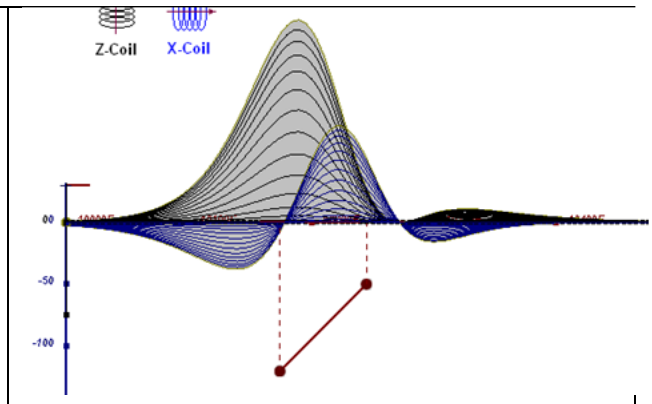
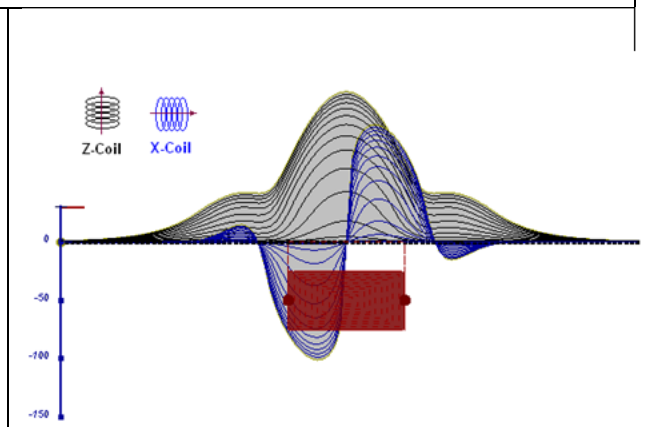**Figure D-2**: inclined thin plate
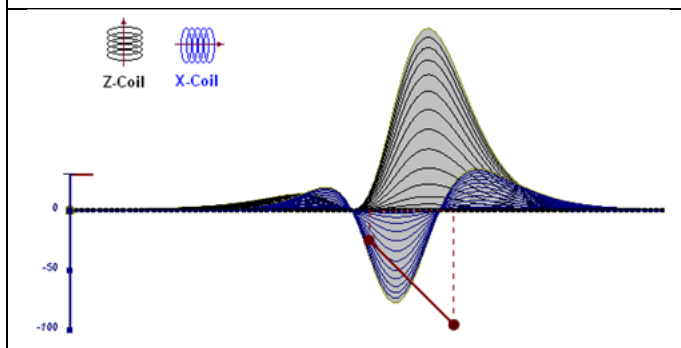
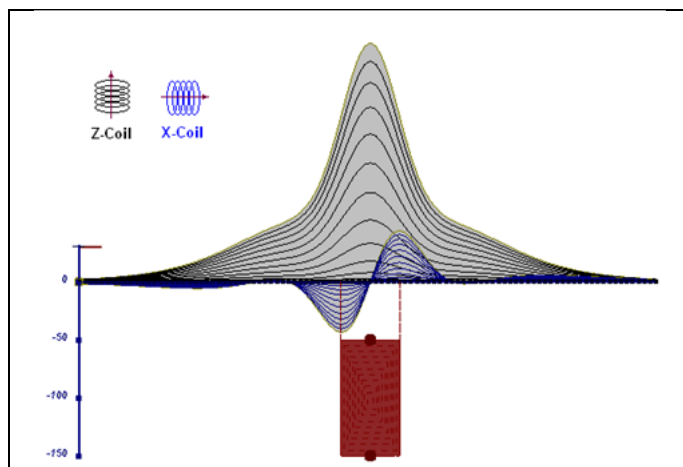**Figure D-3**: inclined thin plate
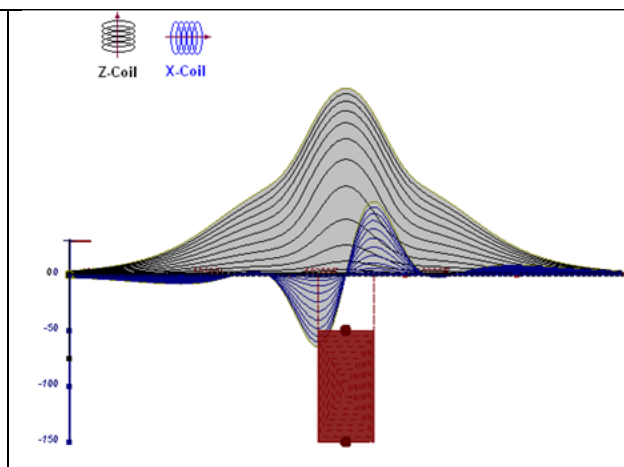

Figure D-4: horizontal thin plate

Figure D-5: horizontal thick plate (linear scale of the response)
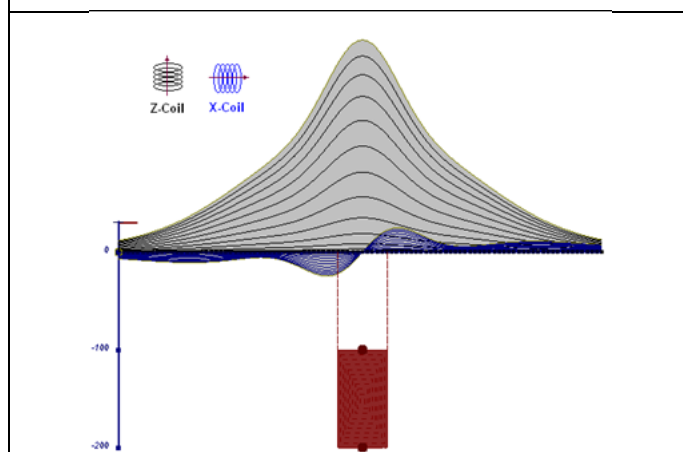

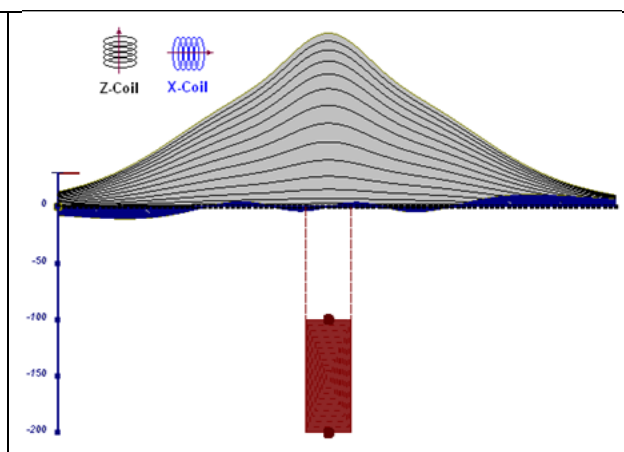**Figure D-6**: horizontal thick plate (log scale of the response)

Figure D-7: vertical thick plate (linear scale of the response). 50 m depth
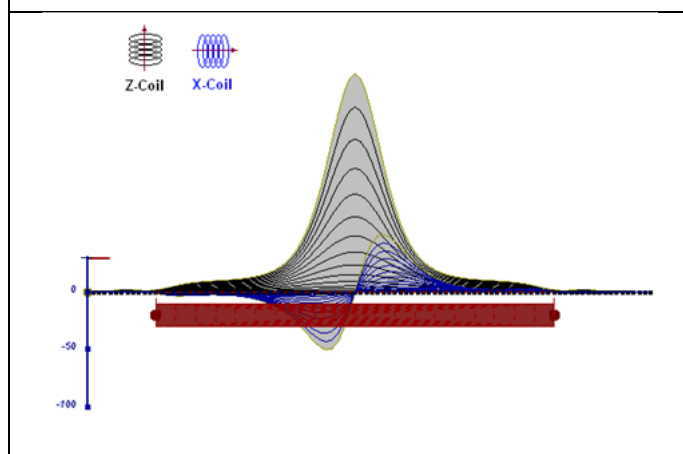

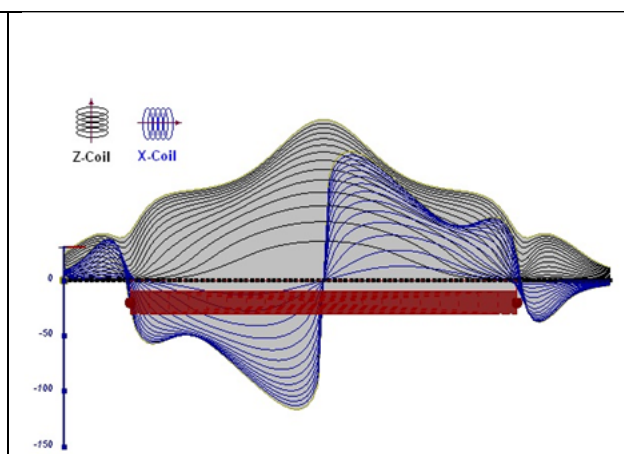**Figure D-8**: vertical thick plate (log scale of the response). 50 m depth

Figure D-9: vertical thick plate (linear scale of the response). 100 m depth

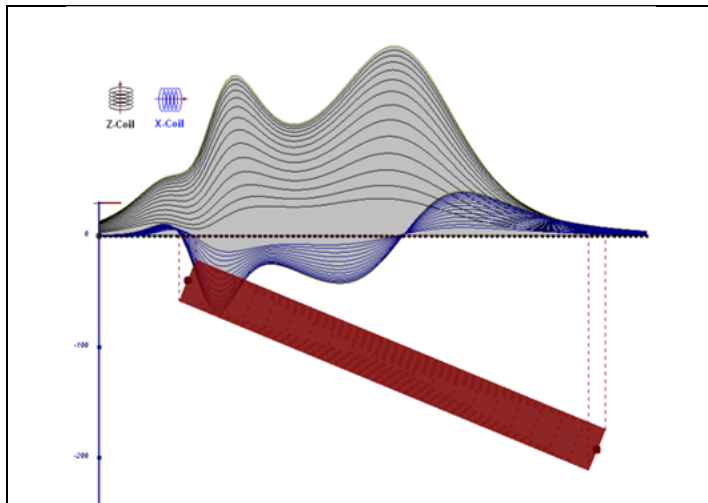**Figure D-10**: vertical thick plate (linear scale of the response). Depth / horizontal thickness=2.5

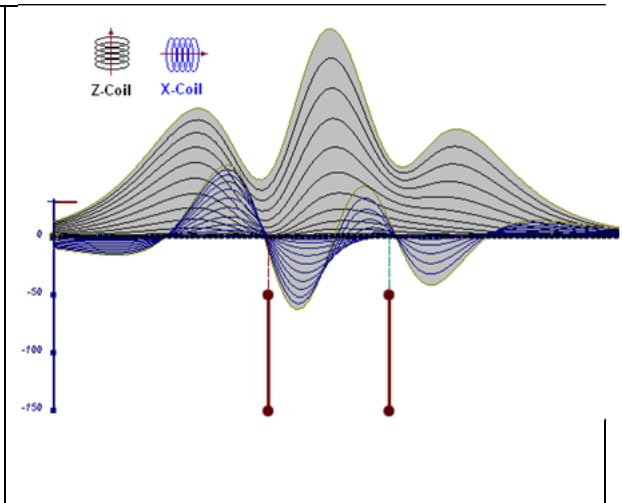**Figure D-11**: horizontal thick plate (linear scale of the response)

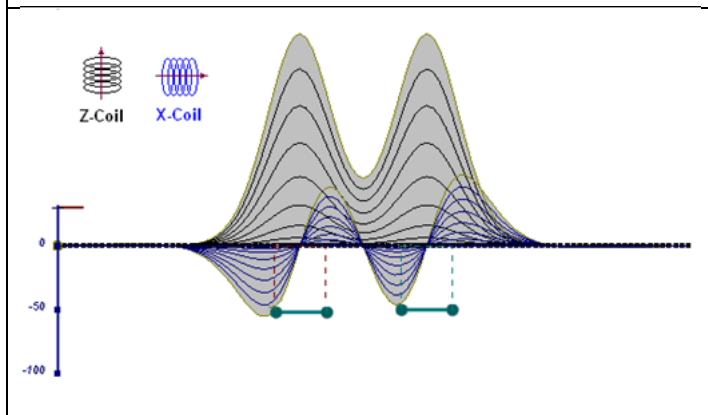**Figure D-12**: horizontal thick plate (log scale of the response)

GEOTECH
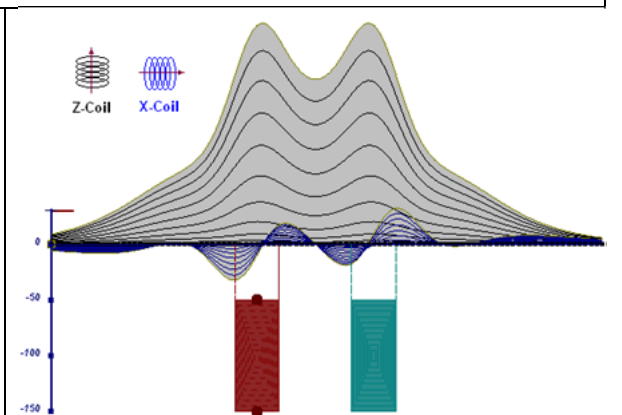AIRBORNE GEOPHYSICAL SURVEYS

Figure D-13: inclined long thick plate

Figure D-14: two vertical thin plates

Figure D-15: two horizontal thin plates

Figure D-16: two vertical thick plates

GEOTECH
AIRBORNE GEOPHYSICAL SURVEYS

The same type of target but with different thickness, for example, creates different form of the response:

| "thin" | 10 m thickness | 15 m thickness |
| 18 m thickness | 20 m thickness | 30 m thickness |
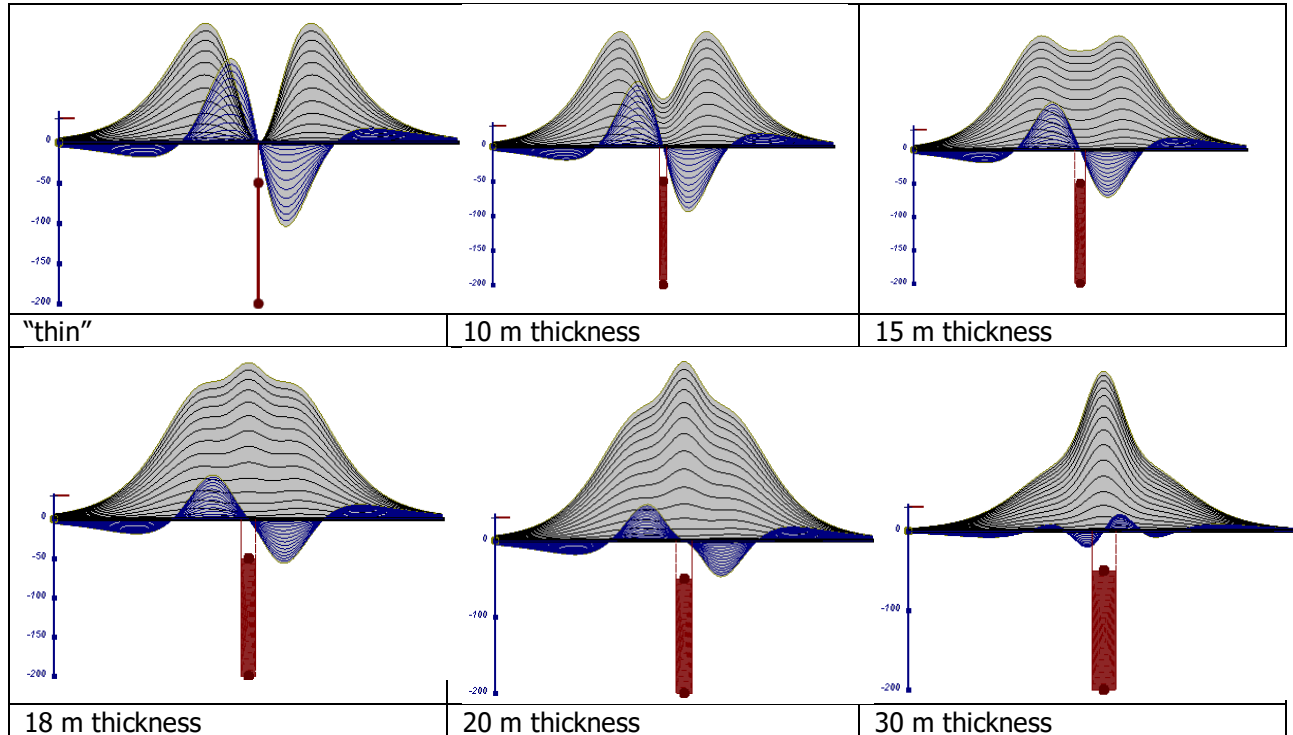
Figure D-17: Conductive vertical plate, depth 50 m, strike length 200 m, depth extends 150 m.

Alexander Prikhodko, PhD, P.Geo
Geotech Ltd.

September 2010